UCRL-11047

University of California

Ernest O. Lawrence Radiation Laboratory

HYPERFINE STRUCTURES AND ANOMALY OF Li^6 AND Li^7 AND THE HYPERFINE STRUCTURES OF Re^{186} AND Re^{188}

Berkeley, California

DISCLAIMER

UCRL-11047
UC-34 Physics
TID-4500 (19th Ed.)

UNIVERSITY OF CALIFORNIA

Lawrence Radiation Laboratory
Berkeley, California

AEC Contract No. W-7405-eng-48

HYPERFINE STRUCTURES AND ANOMALY OF Li^6 AND Li^7, AND THE HYPERFINE STRUCTURES OF Re^{186} AND Re^{188}

Richard G. Schlecht
(Thesis)

October 3, 1963

HYPERFINE STRUCTURES AND ANOMALY OF Li^6 AND Li^7 AND THE HYPERFINE STRUCTURES OF Re^{186} AND Re^{188}

Contents

constants of Re^{186} we obtained

$$a_{186} = \pm 78.3058(24) \text{ Mc/sec} ,$$

and

$$b_{186} = \mp\ 8.3601(50) \text{ Mc/sec} .$$

Therefore, for these hyperfine-structure separations we have

$$\Delta\nu_{186}(7/2,\ 5/2) = \pm 265.292(14) \text{ Mc/sec} ,$$

and

$$\Delta\nu_{186}(5/2,\ 3/2) = \pm 208.305(14) \text{ Mc/sec} .$$

For the interaction constants of Re^{188} we obtained

$$a_{188} = \pm 80.4320(32) \text{ Mc/sec} ,$$

and

$$b_{188} = \mp\ 7.7455(60) \text{ Mc/sec} .$$

Therefore, for these two hyperfine-structure separations we have

$$\Delta\nu_{188}(7/2,\ 5/2) = \pm 273.379(13) \text{ Mc/sec} ,$$

and

$$\Delta\nu_{188}(5/2,\ 3/2) = \pm 212.698(17) \text{ Mc/sec} .$$

The nuclear moments of both isotopes were determined to be positive. An improved value for the electronic Landé g factor for rhenium was also obtained, with the result

$$g_J = -1.95203(8) .$$

HYPERFINE STRUCTURES AND ANOMALY OF Li^6 AND Li^7, AND THE HYPERFINE STRUCTURES OF Re^{186} AND Re^{188}

Richard G. Schlecht

Lawrence Radiation Laboratory
University of California
Berkeley, California

October 3, 1963

ABSTRACT

The atomic-beam magnetic-resonance flop-in technique has been used to determine the hyperfine-structure separations and the hyperfine-structure anomaly between the isotopes Li^6 and Li^7; this technique has also been used to measure the hyperfine-structure separations of the isotopes Re^{186} and Re^{188}.

The separated-oscillatory-field method of Ramsey was used to very accurately determine the hyperfine-structure separations in Li^6 and Li^7. The result for Li^6 is

$$\Delta\nu_6 = 228.20528(8) \text{ Mc/sec} ,$$

and for Li^7 is

$$\Delta\nu_7 = 802.50404(48) \text{ Mc/sec} .$$

By using these values and the value for the ratio of the g_I's as obtained by Klein, the hyperfine-structure anomaly was determined to be

$$_6\Delta_7 = +1.065(6) \times 10^{-4} .$$

The errors quoted are four times the statistical errors.

The magnetic-dipole-interaction constant, a, and the electric-quadrupole-interaction constant, b, have been measured for two radioactive isotopes of rhenium in the $J = 5/2$ ground state. Beams were produced by electron bombardment of irradiated rhenium wires. The spins of both isotopes had been determined previously to be one. For the interaction

I. INTRODUCTION

In this paper we describe two independent experiments using the atomic-beam magnetic-resonance flop-in technique. A different atomic-beam machine was used for each experiment.

The first experiment involved the measurement of the hyperfine structures of the two stable isotopes of lithium, Li^6 and Li^7; the great accuracy of these measurements enabled us to determine a value for the hyperfine-structure anomaly between the two isotopes. This experiment is described in Sec. V. The atomic-beam machine used in this experiment was recently built by the group at Berkeley and is still being modified. As it has not been previously described, it is discussed in Sec. IV. However, work still in progress on the application of the existing theories of hyperfine-structure anomalies to the lithium problem is not discussed.

The second experiment, involving the measurement of the hyperfine structures of two of the radioactive isotopes of rhenium, is discussed in Sec. VI. In the past, it has proven difficult to produce beams of refractory elements for atomic-beam investigations. Therefore, the method of beam production is delineated in this section. Rhenium lies in a region of large nuclear deformation and its nuclear properties should be a good test of the collective model of the nucleus.

A brief description of the theory of electronic structure is given in Sec. II. The theory of hyperfine structures and the Bohr-Weisskopf theory of hyperfine-structure anomalies are also discussed. Additionally, in Sec. II we briefly describe the basic principles of the atomic-beam method and give references about more detailed expositions.

II. THEORY

A. Electronic Structure

The approximate electronic Hamiltonian is given by

$$\mathcal{H} = \sum_{i=1}^{N} \left[\frac{\underset{\sim}{p}_i^2}{2m} - \frac{Ze^2}{r_i} + \xi(r_i)\, \underset{\sim}{\ell}_i \cdot \underset{\sim}{s}_i \right] + \sum_{i>j=1}^{N} \frac{e^2}{r_{ij}} + \mathcal{H}_{hfs} , \qquad (2.1)$$

where the summations extend over the total number of electrons in the atom.[1] The first term in the single summation represents the kinetic energy of the individual electrons, the second the Coulomb interaction of each electron with the nucleus. The third term is the interaction of each electron's spin moment with its own orbital moment. The double summation denotes the Coulombic repulsion of each electron with each of the other electrons, counted once. The final term represents the interaction of the electrons with the multipole fields of order greater than zero produced by the nucleus. In this paper we are primarily concerned with this final term. The above Hamiltonian is nonrelativistic and ignores spin-spin, spin-other-orbit, and orbit-orbit interactions.

The usual method for solving this Hamiltonian is by a perturbation procedure. It is assumed that each electron moves in a central field $U(r_i)$ that is produced by the other electrons and the nucleus. Then the zero-order Hamiltonian,

$$\mathcal{H}_0 = \sum_{i=1}^{N} \left[\frac{\underset{\sim}{p}_i^2}{2m} + U(r_i) \right] ,$$

is separable. To obtain the potential $U(r_i)$ and the wavefunctions, which diagonalize $\mathcal{H}_0$, we make an "educated guess" of a product of single electron wavefunctions (Hartree) or an antisymmetrized product (Hartree-Fock). With this "guess" we then calculate

$$U(r_i) = -\frac{Ze^2}{r_i} + \left\langle \sum_{j \neq i} \frac{e^2}{r_{ij}} \right\rangle_{av} . \qquad (2.2)$$

Putting this into the Schrödinger equation $\mathcal{H}_0 \psi_0 = E_n \psi_0$, we numerically integrate it, obtaining new wavefunctions that are used to recalculate

$U(r_i)$. This process is repeated until "self-consistency" of the wavefunction and $U(r_i)$ is reached. Having obtained the wavefunctions we can calculate the energy of the perturbing Hamiltonian $\mathcal{H}_1$:

$$\mathcal{H}_1 = \sum_{i=1}^{N} \left[-\frac{Ze^2}{r_i} - U(r_i) \right] + \sum_{i>j=1}^{N} \frac{e^2}{r_{ij}}, \qquad (2.3)$$

where the spin-orbit interaction and the hyperfine-structure term, $\mathcal{H}_{hfs}$, have been neglected. For the heavier elements this approximation is not valid, since the spin-orbit term becomes comparable to or larger than the Coulombic repulsion term. However, for most elements, this is a valid approximation. We evaluate the eigenvalues and eigenfunctions of this perturbing Hamiltonian by solving the secular equation $|(\mathcal{H}_0 + \mathcal{H}_1)_{ij} - E\delta_{ij}| = 0$, using the previously determined eigenfunctions. By perturbation theory, the eigenvalues and eigenfunctions of the spin-orbit term can then be determined. Following this scheme we would obtain an energy-level diagram similar to that depicted in Fig. 1. The degree of degeneracy and the Hamiltonian involved in each splitting are also shown.

B. Hyperfine Structure

Since the treatment of hyperfine structure by Schwartz[2] is well known and complete, my general treatment of this topic is brief.

Schwartz first demonstrates how the electric and magnetic interactions of an orbital electron with the nucleus can be expressed in tensor form. It is easily shown that the electrostatic potential of the nucleus can be written

$$V(\underset{\sim}{r}) = \int \frac{\rho(r')}{|\bar{r} - \bar{r}'|} d\tau'$$

$$= \sum_{k=1}^{\infty} r_>^{-k-1} C^{(k)}(\theta, \phi) \cdot \left[Ze \int \psi^* r_<^k C^{(k)}(\theta', \phi') \psi d\tau' \right] \qquad (2.4)$$

$$= \sum_{k=1}^{\infty} r^{-k-1} C^{(k)}(\theta, \phi) \cdot Q_k,$$

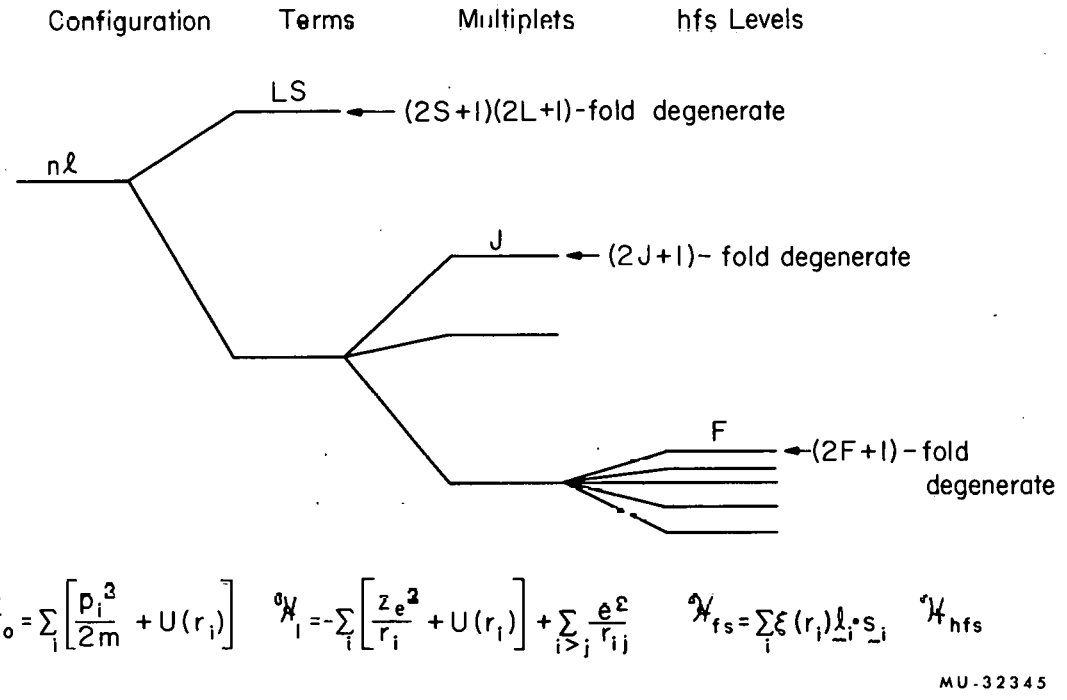

Fig. 1. Degree of degeneracy and the Hamiltonian involved of the atomic energy levels.

where $C_\mu^{(k)}(\theta, \phi) = \left(\frac{4\pi}{2k+1}\right)^{\frac{1}{2}} Y_{k\mu}(\theta, \phi)$, and where it is assumed that $r_>$ always corresponds to the electron's coordinates or that the nucleus is a point and is of infinite mass. We define Q_k as the nuclear-electric multipole moment of order k, which depends only on the nuclear coordinates. For the magnetic-vector potential it is more difficult to show that

$$\underset{\sim}{A}(\underset{\sim}{r}) = -\sum_{k=1}^{\infty} \frac{i\mu_N}{k(k+1)} \left[\underset{\sim}{O} C^{(k)}(\theta, \phi)\right] \cdot \left\{ r_>^{-k-1} \int \psi^* \left[\nabla r_<^k C^{(k)}(\theta', \phi') \cdot (2g_\ell \underset{\sim}{L} + (k+1) g_s \underset{\sim}{S}) \right] \psi d\tau' \right\}, \tag{2.5}$$

where $\underset{\sim}{O} = -i\underset{\sim}{r} \times \nabla$, and where we have written

$$2g_\ell \mu_N \underset{\sim}{L} \equiv \sum_{i=1}^{Z} g_{\ell_i} \frac{e\hbar}{m_i c} \underset{\sim}{L}_i$$

with the summation extending over the protons, and where we have

$$g_s \mu_N \underset{\sim}{S} \equiv \sum_{i=1}^{N} g_{s_i} \frac{e\hbar}{2m_i c} \underset{\sim}{S}_i$$

with the summation extending over all the nucleons. This expression for the vector potential follows from the same assumptions that were used in determining the scalar potential. Defining M_k, the general nuclear-magnetic multipole moment of order k, in terms of the above integral, we can write

$$\underset{\sim}{A}(\underset{\sim}{r}) = -\sum_{k=1}^{\infty} \frac{i}{k} r^{-k-1} \left[\underset{\sim}{O} C^{(k)}(\theta, \phi)\right] \cdot M_k . \tag{2.6}$$

These potentials are used in the perturbing Hamiltonian of the Dirac equation

$$\mathcal{H}_{hfs} = -e(V - V_e) + e\,\underset{\sim}{\alpha} \cdot \underset{\sim}{A}, \tag{2.7}$$

where V_e is the Coulomb potential and $\underset{\sim}{\alpha}$ is three of the Dirac matrices

$$\underset{\sim}{a} = \begin{pmatrix} 0 & \underset{\sim}{\sigma} \\ \underset{\sim}{\sigma} & 0 \end{pmatrix}.$$

The perturbing Hamiltonian is then in the tensor form,

$$\mathcal{H}_{hfs} = \sum_k T_e^{(k)} \cdot T_n^{(k)} , \tag{2.8}$$

where $T_e^{(k)}$ is a tensor of rank k that depends only on the electronic coordinates, and $T_n^{(k)}$ is a tensor of rank k that depends only on the nuclear coordinates.

Note that the operator Q_k has parity $(-1)^k$ and M_k has parity $(-1)^{k+1}$, so that only electric moments of even parity and magnetic moments of odd parity exist if the nucleus is assumed to have a well-defined parity.

To the first order in an IJF representation we obtain, for the expectation value of $\mathcal{H}_{hfs}$,

$$W_F = \left\langle IJF \left| \mathcal{H}_{hfs} \right| IJF \right\rangle = \sum_k \left\langle IJF \left| T_e^{(k)} \cdot T_n^{(k)} \right| IJF \right\rangle = \sum_k \frac{(-1)^{I+J-F} W(IJIJ;Fk)}{(2J)!\,(2I)!}$$
$$\cdot \left[(2J-k)!\,(2J+k+1)!\,(2I-k)!\,(2I+k+1)! \right]^{\frac{1}{2}} \cdot A_k , \tag{2.9}$$

where W(IJIJ;Fk) is the Racah coefficient, the values of which have been tabulated.[3] The first three A's are related to the usual hyperfine-structure interaction constants by

$$A_1 = IJa, \quad A_2 = \frac{1}{4} b, \quad \text{and} \quad A_3 = c . \tag{2.10}$$

Taking the first three terms, we obtain

$$W_F = \frac{K}{2} a + \frac{3b}{4} \frac{[K(K+1) - 4/3\, I(I+1)J(J+1)]}{2I(2I-1)J(2J-1)}$$
$$+ 5c \left[K^3 + 4K^2 + \frac{4}{5} K\{-3I(I+1)J(J+1) + I(I+1) + 3\} \right. \tag{2.11}$$
$$\left. - 4I(I+1)J(J+1) \right] \frac{1}{4I(I-1)(2I-1)J(J-1)(2J-1)} ,$$

where $K = F(F+1) - I(I+1) - J(J+1)$. The hyperfine-structure separation between two levels F and F' is given by

$$\Delta\nu(F, F') = W_F(F) - W_F(F') , \qquad (2.12)$$

where a, b, c and $\Delta\nu$ are in the same units.

C. Effect of an External Magnetic Field

The effect of adding an external magnetic field $\underset{\sim}{H}_0$ to an atom is to add two terms to the total Hamiltonian. These are

$$\mathcal{H}_{ext} = -g_J\mu_0 J_z H_0 - g_I\mu_0 I_z H_0 . \qquad (2.13)$$

The first term describes the interaction of the external field with the magnetic-dipole moment of the orbital electrons. The second term describes the interaction of the external field with the magnetic-dipole moment of the nucleus. There are two cases in which this interaction is easily calculated. These are when

$$x = \frac{(g_I - g_J)\mu_0 H_0}{h\Delta\nu} \ll 1 ,$$

and when

$$\frac{(g_I - g_J)\mu_0 H_0}{h\Delta\nu} \gg 1 .$$

In the weak field case ($x \ll 1$), I and J remain coupled and precess about F. This gives rise to an effective moment

$$\underset{\sim}{\mu}_{eff} = g_J\mu_0 \frac{\underset{\sim}{J}\cdot\underset{\sim}{F}}{\underset{\sim}{F}\cdot\underset{\sim}{F}} \underset{\sim}{F} + g_I\mu_0 \frac{\underset{\sim}{I}\cdot\underset{\sim}{F}}{\underset{\sim}{F}\cdot\underset{\sim}{F}} \underset{\sim}{F} , \qquad (2.14)$$

which precesses about $\underset{\sim}{H}_0$. The interaction energy due to the external field is given by

$$W_{ext} = -\underset{\sim}{\mu}_{eff}\cdot\underset{\sim}{H}_0 = -g_F\mu_0 m_F H_0 , \qquad (2.15)$$

where

$$g_F = g_J \frac{F(F+1) + J(J+1) - I(I+1)}{2F(F+1)} + g_I \frac{F(F+1) - J(J+1) + I(I+1)}{2F(F+1)} .$$

In the strong-field case ($x \gg 1$), I and J are decoupled and precess independently about $\underset{\sim}{H}_0$. In this case $\mathcal{H}_{ext}$ is diagonal in an IJm_Im_J representation and we obtain for the energy due to the external

field

$$W_{ext} = -g_J \mu_0 m_J H_0 - g_I \mu_0 m_I H_0 . \qquad (2.16)$$

These two types of coupling are depicted schematically in Fig. 2.

We can easily diagonalize $\mathcal{H}_{ext}$ for the intermediate fields as well, when I or J is equal to one-half. This is the case with lithium, where $J = 1/2$. Assuming that I and J are good quantum numbers, we need only diagonalize a 2×2 matrix. For the hyperfine-structure Hamiltonian with an external field we have

$$\mathcal{H}_{1/2} = \mathcal{H}_{hfs} + \mathcal{H}_{ext} = a \underset{\sim}{I} \cdot \underset{\sim}{J} - g_J \mu_0 J_z H_0 - g_I \mu_0 I_z H_0 . \qquad (2.17)$$

The quadratic equation that results from the diagonalization can be solved to yield the well-known Breit-Rabi equation[4,5]

$$W = -\frac{\Delta W}{2(2I+1)} - g_I \mu_0 m_F H_0 \pm \frac{\Delta W}{2} \left(1 + \frac{4 m_F x}{2I+1} + x^2 \right)^{\frac{1}{2}} , \qquad (2.18)$$

where $\Delta W = a \frac{(2I+1)}{2}$ and

$$x = \frac{(g_I - g_J)\mu_0 H_0}{\Delta W} .$$

The positive sign refers to the state $\left| F = I + 1/2, m_F \right\rangle$ and the negative sign to the state $\left| F = I - 1/2, m_F \right\rangle$ and to the state $\left| F = I + 1/2, m_F = -I - 1/2 \right\rangle$ when $x \gtrsim \frac{2I}{2I+1}$.

D. Hyperfine-Structure Anomalies--Bohr-Weisskopf Theory

As was shown earlier, an atom with $J = 1/2$ can have only magnetic-dipole interactions and no higher-order multipole moments. For an atom with an unpaired s electron the magnetic-dipole interaction constant can be easily calculated. Many derivations have been given.[5-8]

Assuming that I and J are good quantum numbers, the nuclear and electronic dipole moments can be written

$$\underset{\sim}{\mu_I} = g_I \mu_0 \underset{\sim}{I} \quad \text{and} \quad \underset{\sim}{\mu_J} = g_J \mu_0 \underset{\sim}{J} , \qquad (2.19)$$

where g_I and g_J are the nuclear and electronic Landé g factors,

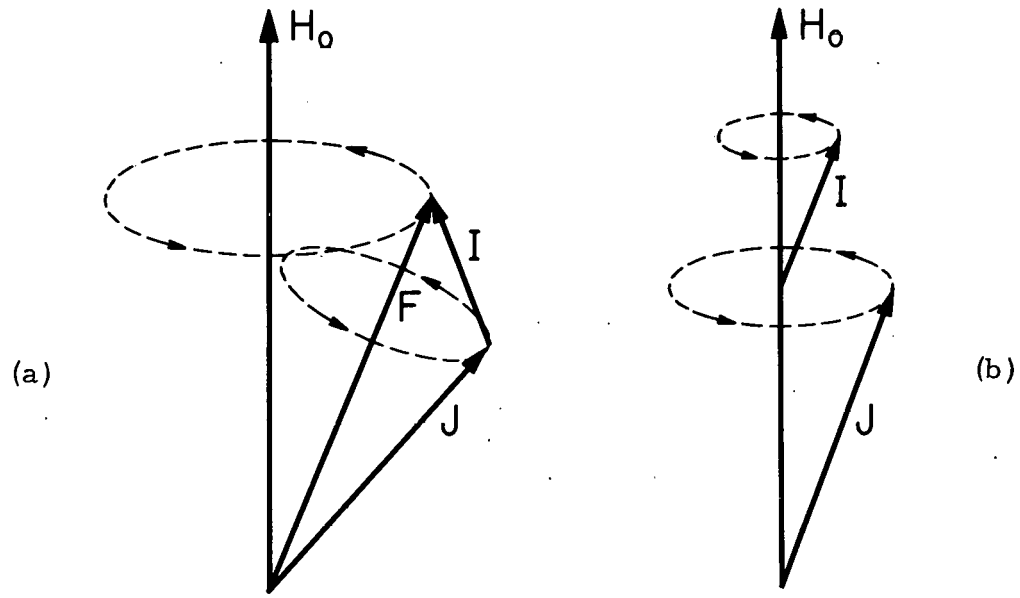

Fig. 2. Precession of $\underset{\sim}{I}$, $\underset{\sim}{J}$ and $\underset{\sim}{F}$ in (a) a weak magnetic field, and (b) a strong magnetic field.

respectively, and μ_0 is the Bohr magneton. Then, for the vector potential of the nucleus, we have

$$\underset{\sim}{A}_n(\underset{\sim}{r}) = -\underset{\sim}{\mu}_I \times \nabla \frac{1}{r} = -g_I \mu_0 \underset{\sim}{I} \times \nabla \frac{1}{r}, \qquad (2.20)$$

where the nucleus is at the origin. First we take the curl of $\underset{\sim}{A}_n$ to obtain the magnetic field. Then we take the negative dot product of the magnetic field with the electronic-dipole moment to obtain the Hamiltonian,

$$\mathcal{H} = g_I g_J \mu_0^2 \, \underset{\sim}{J} \cdot \nabla \times \left(\underset{\sim}{I} \times \nabla \frac{1}{r} \right). \qquad (2.21)$$

Expanding, we have

$$\mathcal{H} = g_I g_J \mu_0^2 \, \underset{\sim}{I} \cdot \underset{\sim}{J} \, \nabla^2 \frac{1}{r} - g_I g_J \mu_0^2 \, (J \cdot \nabla)(I \cdot \nabla) \frac{1}{r}. \qquad (2.22)$$

The second term splits into a spherically symmetric part, $-1/3 \, g_I g_J \mu_0^2 \, \underset{\sim}{I} \cdot \underset{\sim}{J} \, \nabla^2 \frac{1}{r}$, and a term which is purely angular dependent. Since the s state is spherically symmetric the angular dependent term averages to zero and so will be ignored. Now, since we have $\nabla^2 (1/r) = -4\pi \, \delta(\underset{\sim}{r})$, where $\delta(\underset{\sim}{r})$ is the Dirac delta function, we obtain for the Hamiltonian

$$\mathcal{H} = \frac{2}{3} g_I g_J \mu_0^2 \, \underset{\sim}{I} \cdot \underset{\sim}{J} \, \nabla^2 \frac{1}{r} = -\frac{8\pi}{3} g_I g_J \mu_0^2 \, \underset{\sim}{I} \cdot \underset{\sim}{J} \, \delta(\underset{\sim}{r}). \qquad (2.23)$$

Therefore, the energy is given by

$$W = -\frac{8\pi}{3} g_I g_J \mu_0^2 \, \underset{\sim}{I} \cdot \underset{\sim}{J} \, |\psi(0)|^2 = a \, \underset{\sim}{I} \cdot \underset{\sim}{J}, \qquad (2.24)$$

where $\psi(0)$ is the value of the electron wavefunction at the nucleus. This Fermi formula and various corrections to it were calculated by many authors, and the results have been tabulated by Kopfermann.[9] For s electrons of alkali atoms, one obtains

$$a = -\frac{8}{3} \frac{g_I g_J \mu_0^2 Z Z_0^2}{n_0^3 a_0^3} \left(1 + \frac{m}{M_n}\right)^{-3} \left(1 - \frac{d\sigma}{dn}\right) F_r(J, Z)(1 - \delta)(1 - \epsilon), \qquad (2.25)$$

where: m = mass of electron; M_n = mass of the nucleus; a_0 = Bohr radius;

Z = atomic number of the atom; Z_0 = the effective charge seen by the s electron when outside all electron shells; $\left(1 - \frac{d\sigma}{dn}\right)$ = the Fermi-Segrè factor[10] (which arises from the inclusion in the calculation of $|\psi(0)|^2$ of all four components of the Dirac wave functions); $n_0 = n - \sigma$, the effective principal quantum number of the electron, σ being the Rydberg correction; $F_r(J, Z)$ = a relativistic correction factor (≈ 1) calculated by Casimir[11] and tabulated by Kopfermann[9]; $(1 - \delta)$ = the Breit-Rosenthal correction[12-14] due to the finite extent of the nuclear charge; and $(1 - \epsilon)$ = the Bohr-Weisskopf correction[15,16] due to the finite extent of the nuclear magnetism.

We have included in this formula an effect due to the nuclear motion, the term $\left(1 + \frac{m}{M_n}\right)^{-3}$, which is not given in Kopfermann's expression. This effect was calculated by Breit and Meyerott.[17]

Besides g_I, the only factors in Eq. (2.25) that depend on nuclear properties are the Breit-Rosenthal correction, the Bohr-Weisskopf correction, and the nuclear-motion correction. Taking the ratio of the a factors of two isotopes, we obtain

$$\frac{a_1}{a_2} = \frac{g_{I_1}(1 - \delta_1)(1 - \epsilon_1)}{g_{I_2}(1 - \delta_2)(1 - \epsilon_2)} \left(\frac{\mu_1}{\mu_2}\right)^3 , \qquad (2.26)$$

where μ_1 and μ_2 are the reduced masses of isotope one and two, respectively. Neglecting the Breit-Rosenthal correction and the Bohr-Weisskopf correction, we obtain the well-known Fermi-Segrè formula,

$$\frac{\Delta\nu_1}{\Delta\nu_2} = \frac{g_{I_1}(2I_1 + 1)}{g_{I_2}(2I_2 + 1)} \left(\frac{\mu_1}{\mu_2}\right)^3 , \qquad (2.27)$$

where $\Delta\nu$ is the hyperfine-structure separation of the respective isotope. The hyperfine-structure anomaly, Δ, is defined as

$$\left(\frac{\Delta\nu_1}{\Delta\nu_2}\right)_{calc} = \left(\frac{\Delta\nu_1}{\Delta\nu_2}\right)_{obs} (1 - {}_1\Delta_2) , \qquad (2.28)$$

and

$${}_2\Delta_1 \approx - {}_1\Delta_2 ,$$

where $\left(\frac{\Delta\nu_1}{\Delta\nu_2}\right)_{calc}$ is the ratio of the hyperfine structures as calculated from the Fermi-Segrè formula and $\left(\frac{\Delta\nu_1}{\Delta\nu_2}\right)_{obs}$ is the observed ratio. From this we see that

$$(1 - {}_1\Delta_2) = \frac{(1-\delta_2)(1-\epsilon_2)}{(1-\delta_1)(1-\epsilon_1)} . \qquad (2.29)$$

Therefore, to calculate Δ, we must determine the δ's and ϵ's. However, we can account for the Breit-Rosenthal correction in a determination of the ϵ's by modifying the electronic wavefunctions in a manner to be discussed in this section.

For a determination of the Bohr-Weisskopf correction we must calculate the energy due to the nuclear magnetism. In order to do this we must first determine the magnetic-vector potential resulting from the nucleus. The magnetic-vector potential arises from two sources: that produced by the spins of the nucleons, and that caused by the orbital motion of the protons. We can write the vector potential due to the spins as

$$\underset{\sim}{A}_S(\underset{\sim}{r}) = -\int d\tau_n\, \omega(\underset{\sim}{R}) g_s \left(\underset{\sim}{S} \times \nabla_r \frac{1}{|\underset{\sim}{r} - \underset{\sim}{R}|}\right), \qquad (2.30)$$

where

$$\int \omega(\underset{\sim}{R}) d\tau_n = 1 .$$

The integral extends over the nuclear volume, $\omega(\underset{\sim}{R})$ is the magnetic dipole-moment density of the nucleus, $\underset{\sim}{S}$ is the nuclear-spin angular momentum, and g_s is the spin g factor. The magnetic-vector potential due to the orbital motion of the protons can be written

$$\underset{\sim}{A}_L(\underset{\sim}{r}) = \frac{1}{c}\int \frac{\underset{\sim}{j}}{|\underset{\sim}{r} - \underset{\sim}{R}|} d\tau_n = \frac{Ze}{M_n c}\int \psi_n^* \frac{\underset{\sim}{p}}{|\underset{\sim}{r} - \underset{\sim}{R}|} \psi_n d\tau_n , \qquad (2.31)$$

where $\underset{\sim}{j}$ is the current distribution due to the protons, and ψ_n is the nuclear wavefunction. The integral again extends over the nuclear volume. For the perturbation Hamiltonian due to the nuclear magnetization we have

$$\mathcal{H}_3 = e\,\underset{\sim}{\alpha}\cdot\underset{\sim}{A} = e\,\underset{\sim}{\alpha}\cdot[\underset{\sim}{A}_S(\underset{\sim}{r}) + \underset{\sim}{A}_L(\underset{\sim}{r})] . \qquad (2.34)$$

To the first order in the energy we have

$$W = W_S + W_L = \langle \psi_0 | e\, \underset{\sim}{a} \cdot \underset{\sim}{A}_S(\underset{\sim}{r}) | \psi_0 \rangle + \langle \psi_0 | e\, \underset{\sim}{a} \cdot \underset{\sim}{A}_L(\underset{\sim}{r}) | \psi_0 \rangle , \quad (2.33)$$

where the zero-order wavefunctions ψ_0 are given by[18]

$$\psi_0 = \begin{pmatrix} \psi_{\ell jm} \\ \phi_{\bar{\ell} jm} \end{pmatrix}, \quad \text{where} \quad \bar{\ell} = \ell \pm 1 , \quad (2.34)$$

depending upon whether $j = \ell \pm 1/2$,

$$\psi_{\ell jm} = \frac{f(r)}{r} \mathcal{Y}_{\ell jm}, \quad \text{and} \quad \phi_{\bar{\ell} jm} = \frac{g(r)}{ir} \mathcal{Y}_{\bar{\ell} jm}, \quad (2.35)$$

where $f(r)$ and $g(r)$ are the radial components of the relativistic wavefunctions. The $\mathcal{Y}_{\ell jm}$ is given by

$$\mathcal{Y}_{\ell jm} = \sum_{m_\ell m_s} (1/2\ m_s \ell\, m_\ell \,|\, 1/2\ \ell jm) \cdot Y_{\ell\, m_\ell}(\theta\phi) \chi_{\frac{1}{2} m_s} , \quad (2.36)$$

where $(\frac{1}{2}\ m_s\ \ell\, m_\ell \,|\, \frac{1}{2}\ \ell\ jm)$ is the Wigner coefficient, $Y_{\ell\, m_\ell}$ is the spherical harmonic, and $\chi_{\frac{1}{2} m_s}$ is the usual two-component spinor.

After expanding the expression $\underset{\sim}{a} \cdot \underset{\sim}{A}_S$, using the usual expansion for $\left(\frac{1}{|\underset{\sim}{r} - \underset{\sim}{R}|}\right)$, and integrating over the angular part of the electron's coordinates, we obtain for the energy due to the spin magnetization the expression

$$W_S = \frac{16\pi e}{3} \int d\tau_n \omega(\underset{\sim}{R}) g_s S_z \int_R^\infty \frac{f(r)g(r)}{r^2}\, dr + \frac{16\pi e}{3} \int d\tau_n \omega(\underset{\sim}{R}) g_s \quad (2.37)$$

$$\cdot \left[\frac{3}{2} S_y \frac{Z_n Y_n}{R^5} + \frac{3}{2} S_x \frac{Z_n X_n}{R^5} - \frac{1}{2} S_z \frac{R^2 - 3Z_n^2}{R^5} \right] \int_0^R r f(r) g(r) dr .$$

In the point-dipole approximation we have, for the hyperfine-structure energy due to the spin moment,

$$W_S^0 = \frac{16\pi e}{3} \int d\tau_n \omega(\underset{\sim}{R}) g_s S_z \int_0^\infty \frac{f(r)g(r)}{r^2}\, dr . \quad (2.38)$$

Therefore, if we neglect the asymmetric term, we have

$$W_S = W_S^0 - \frac{16\pi e}{3}\int d\tau_n \omega(\underset{\sim}{R}) g_s S_z \int_0^R \frac{f(r)g(r)}{r^2}\, dr = W_S^0(1 - \langle \kappa_S \rangle), \tag{2.39}$$

where

$$\kappa_S = \left(\int_0^R \frac{fg}{r^2}\, dr\right) \Big/ \left(\int_0^\infty \frac{fg}{r^2}\, dr\right).$$

Therefore, the energy is decreased by an amount $\langle \kappa_S \rangle$. In the same manner we obtain for the energy due to the orbital magnetization the expression

$$W_L = \frac{16\pi e}{3}\int d\tau_n \omega(\underset{\sim}{R}) g_\ell L_z \left[\int_0^R \frac{r}{R^3} f(r)g(r)dr + \int_R^\infty \frac{f(r)g(r)}{r^2}\, dr\right], \tag{2.40}$$

where L_z is the Z component of the nuclear orbital angular momentum of the protons and

$$g_\ell = \frac{Ze\hbar}{2M_n c}.$$

As before, we define a parameter

$$\kappa_L = \left[\int_0^R (r/R^3 - 1/r^2)\, f(r)g(r)dr\right] \Big/ \left[\int_0^\infty \frac{f(r)g(r)}{r^2}\, dr\right].$$

Therefore, we obtain for the energy due to the orbital magnetization of the protons the expression

$$W_L = W_L^0(1 - \langle \kappa_L \rangle), \tag{2.41}$$

where

$$W_L^0 = \frac{16\pi e}{3}\int d\tau_n \omega(\underset{\sim}{R}) g_\ell L_z \int_0^\infty \frac{f(r)g(r)}{r^2}\, dr \tag{2.42}$$

is the hyperfine-structure energy due to the orbital moment in the point-dipole approximation. Therefore, the hyperfine-structure energy due to the orbital moment is decreased by an amount $\langle \kappa_L \rangle$.

One can now include the effects of the finite volume of the nuclear charge. We accomplish this by modifying the Dirac radial wavefunctions f_0 and g_0 as determined by the Coulombic potential. This is done by solving for the potential inside the nucleus produced by the determined nuclear charge density. Solving the Dirac equation for this potential, we obtain new radial wavefunctions f and g. We can fit these functions to the radial wavefunctions f_0 and g_0 at the nuclear surface. This procedure gives

$$\kappa_S = \left(\int_0^R \frac{fg}{r^2}\, dr \right) \Big/ \left(\int_0^\infty \frac{f_0 g_0}{r^2}\, dr \right), \tag{2.43}$$

$$\kappa_L = \left[\int_0^R (r/R^3 - 1/r^2) fg\, dr \right] \Big/ \left(\int_0^\infty \frac{f_0 g_0}{r^2}\, dr \right), \tag{2.44}$$

and

$$W_S^{\,0} = \frac{16\pi e}{3} \int d\tau_n \omega(\underset{\sim}{R}) g_s S_z \int_0^\infty \frac{f_0 g_0}{r^2}\, dr \tag{2.45}$$

and

$$W_L^{\,0} = \frac{16\pi e}{3} \int d\tau_n \omega(\underset{\sim}{R}) g_\ell L_z \int_0^\infty \frac{f_0 g_0}{r^2}\, dr\,. \tag{2.46}$$

If we now let a_S be that fraction of the total hyperfine-structure energy due to the spin moment and a_L that fraction due to the orbital moment, we have

$$\begin{aligned} W &= W_0 \left(1 - a_S \langle \kappa_S \rangle - a_L \langle \kappa_L \rangle\right) \\ &= W_0 (1 - \epsilon)\,, \end{aligned} \tag{2.47}$$

where $\epsilon = a_S \langle \kappa_S \rangle + a_L \langle \kappa_L \rangle$, and where W_0 is the energy in the point-dipole approximation. The a's can be expressed in terms of the g factors so that

$$a_S = \frac{g_S(g_I - g_L)}{g_I(g_S - g_L)}$$

and (2.48)

$$a_L = 1 - a_S .$$

From this we obtain for the hyperfine-structure anomaly

$$_1\Delta_2 = \frac{\epsilon(2) - \epsilon(1)}{1 - \epsilon(1)}, \qquad (2.49)$$

where $\epsilon(1)$ and $\epsilon(2)$ denote the values of ϵ for isotopes one and two, respectively.

III. EXPERIMENTAL METHOD

The measuring of hyperfine structures by the atomic-beam method has not changed significantly since the pioneering work of Rabi[19] and Zacharias.[20] A schematic diagram of the apparatus used is given in Fig. 3. Atoms effusing out of the oven O are deflected by the inhomogeneous A magnet. After collimation, the atoms enter the constant-C-field region where transitions are induced by a radiofrequency hairpin. If the sign of the Z component of the electronic-magnetic moment is reversed by this transition the inhomogeneous B magnet will deflect the atom around the stopwire S and along path 2. It will then be detected at D. Atoms not undergoing this type of transition will follow trajectory 1 and will be lost. In the A and B field regions, the magnitude of the magnetic field will be such that the strong-field approximation holds and the atom will have an effective moment of approximately

$$\mu_{eff} = g_J \mu_0 m_J .$$

The force on the atom in this region is then given by

$$\underset{\sim}{F} = -\nabla W = -\nabla(-\mu_{eff} H_Z) = g_J \mu_0 m_J \frac{\partial H_Z}{\partial Z} .$$

Usually the magnitudes of the A and B fields can be set so that an atom that undergoes a transition will just clear the stopwire.

The transitions that are induced in the C-field region are governed by the usual quantum-mechanical selection rules for magnetic-dipole radiation.[9] For the weak-field case these are

$$\Delta m_F = 0 \quad \text{with} \quad \Delta F = \pm 1 ,$$

or

$$\Delta m_F = 1 \quad \text{with} \quad \Delta F = 0, \pm 1 .$$

For the strong-field case they are

$$\Delta m_J = 0 \quad \text{with} \quad \Delta m_I = \pm 1 ,$$

or

$$\Delta m_I = 0 \quad \text{with} \quad \Delta m_J = \pm 1 .$$

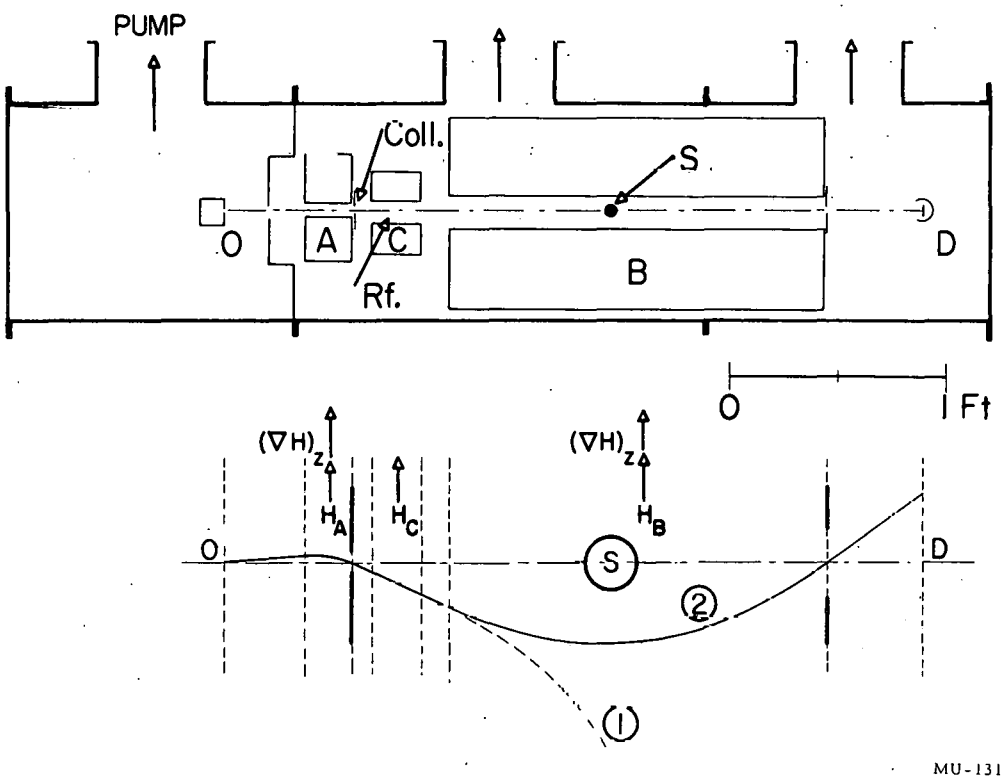

Fig. 3. Schematic diagram of an atomic-beam machine showing possible trajectories.

Since only transitions in which the sign of the Z component of the electronic-magnetic moment is reversed are observable, the number of hyperfine transitions which can be seen by use of the atomic-beam method is greatly reduced. The only transitions observed in the course of this work were those in which $(m_J = +1/2) \longleftrightarrow (m_J = -1/2)$. Transitions where $\Delta F = 0$ will be referred to as Zeeman transitions, and those where $\Delta F = \pm 1$ as direct or hyperfine transitions.

The atomic-beam method is quite well discussed in the literature and the interested reader may wish to consult references 5, 9, 21, and 22.

IV. ATOMIC-BEAM MACHINES

A. Introduction

Two atomic-beam machines were used during the course of the work described herein. For the rhenium experiments, atomic-beam machine A pictured in Fig. 4 was used. This machine was fully described by White[23] and few changes were made. Therefore, no detailed description is given here. For the lithium experiments, atomic-beam machine B pictured in Fig. 5 was used.

B. Atomic-Beam Machine B

1. Geometry

A diagram of atomic-beam machine B is given in Fig. 6. The distances of the important components of the machine from the oven slit are given in Table I. The A, B, and C collimators are externally adjustable in position and width. The position and thickness of the stopwire can also be easily adjusted. The stopwire can also be removed from the beam path.

A calibration oven used to determine the magnitude of the C field is located in the buffer chamber. The Zeeman transition frequency in the calibration isotope is observed and this determines the magnitude of the C field, since the nuclear and electronic properties of this isotope are well known. The buffer oven of atomic-beam machine B was designed for use with cesium-133 as the calibration isotope. Cesium was chosen since the most probable velocity of the cesium atoms in the beam is low. Hence, narrow resonance linewidths can be obtained and therefore the magnitude of the C field can be determined with greater accuracy.

2. Vacuum System

Atomic-beam machine B is evacuated by several oil-diffusion pumps backed by duoseal mechanical pumps. Table II gives a list of the pumps used and their purposes. Between each diffusion pump and the chamber that it evacuates is a liquid nitrogen trap to condense the pump

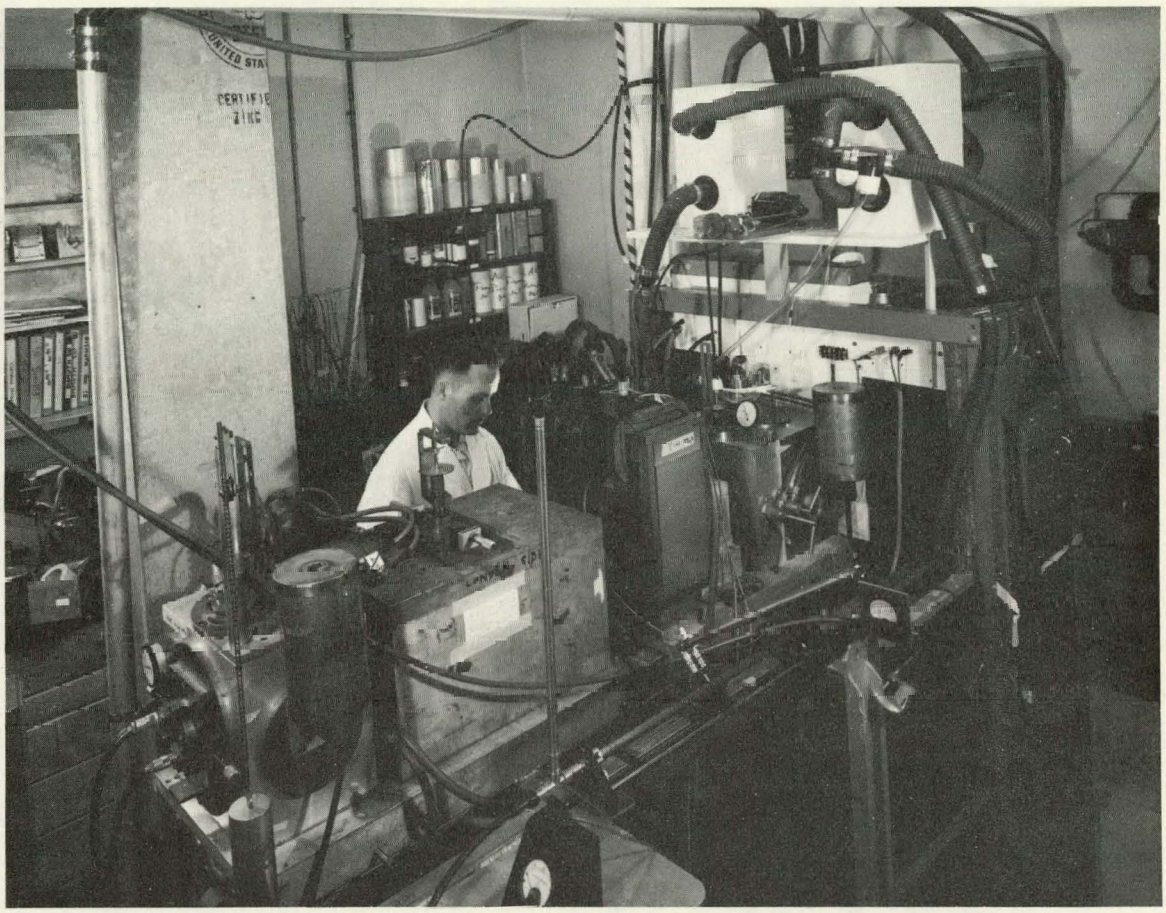

ZN-3401

Fig. 4. Atomic-beam machine A.

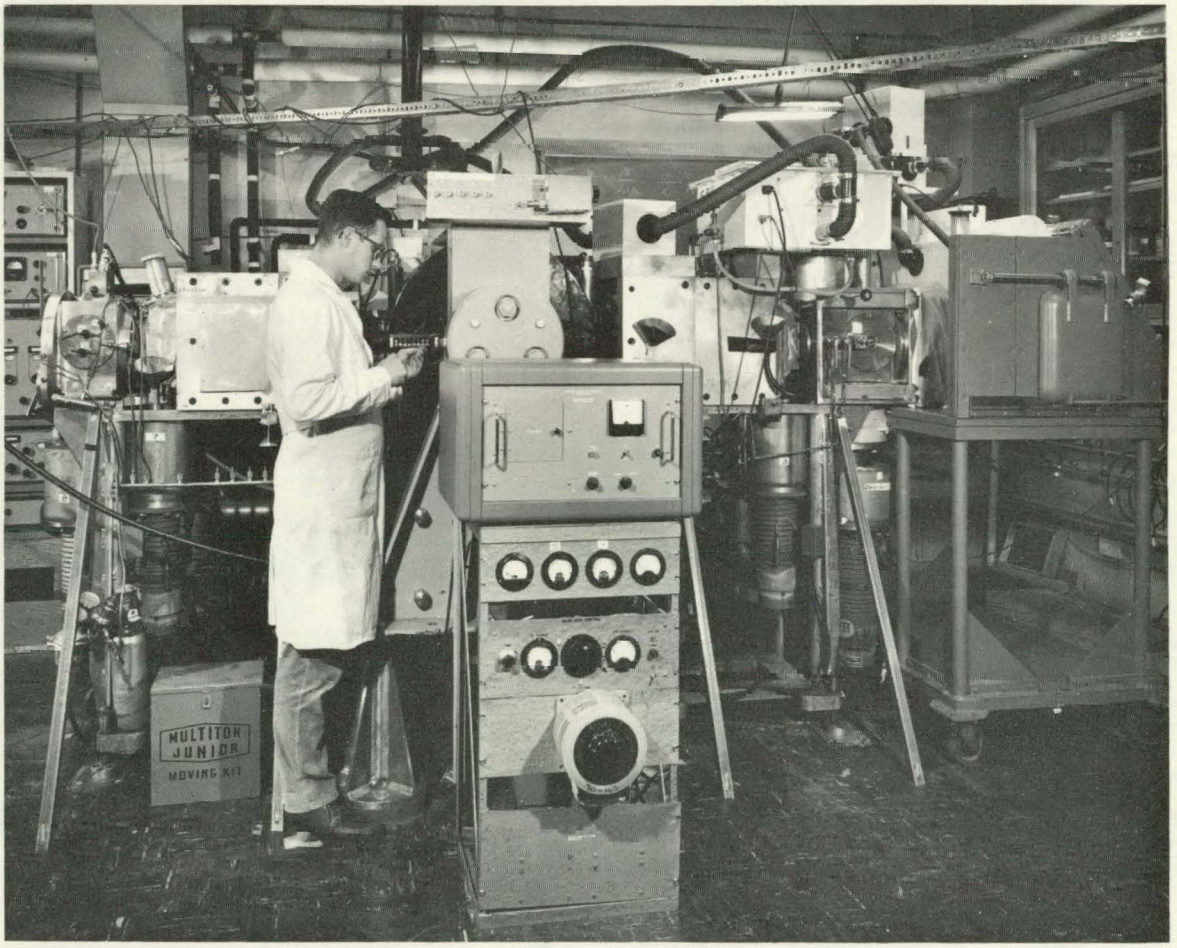

ZN-4005

Fig. 5. Atomic-beam machine B.

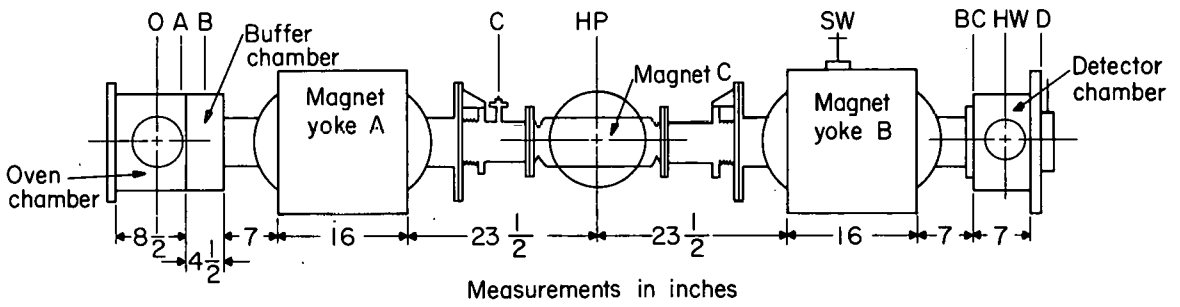

Fig. 6. Diagrammatic sketch of the physical characteristics of atomic-beam machine B.

Table I. Distances of pertinent parts of atomic-beam machine B from oven slit.

Part	Distance from oven slit (in.)
A-collimator and beam chopper	3
Buffer calibration oven	6
C-collimator	42.5
Radiofrequency hairpin	54
Stopwire	85
B-collimator	101
Hotwire detector	104
Foil detector	109

Table II. Pumps used on atomic-beam machine B and their purposes.

Type	Number	Purpose
Diffusion pumps		
CEC-MCF 300 lps	1	evacuates detector chamber
CEC-PMC 720 lps	4	evacuates main can
CEC-MB 100 lps	1	backs main can and detector pumps
CEC-MCF 720 lps	1	evacuates buffer chamber
CEC-PMC 1440 lps	1	evacuates oven chamber
Mechanical pumps		
Welsch 5 cfm	1	backs the CEC-MB diffusion pump
Welsch 3/4 cfm	1	backs the buffer diffusion pump
Welsch 5 cfm	1	backs the oven diffusion pump
Welsch 3/4 cfm	1	evacuates between double sets of "O" rings

oil which escapes and any condensable gases in the system. Pressures of 1×10^{-6} mm of mercury have been obtained with this system.

Sliding valves are situated between the oven and buffer chambers and between the buffer chamber and the main can so that the oven and buffer chambers can each be isolated from the rest of the vacuum system. These chambers, or the main can, may then be brought up to atmospheric pressure individually without losing the vacuum in the rest of the system. The valve system for both the oven and buffer chambers is depicted in Fig. 7. Valves are situated above and below the oven and buffer diffusion pumps so that they can be isolated while the mechanical pumps are "roughing down" the chambers to the sufficient forevacuum pressures needed for the diffusion pumps to function. This avoids the necessity of bringing the diffusion pumps up to atmospheric pressure.

3. Magnet Systems

Since atomic-beam machine B was designed to be symmetrical, the A and B magnets are identical. A cross section of the A and B magnets is given in Fig. 8. The magnet-pole tips are constructed of vanadium permendur and are 21 in. long. The geometry of the pole tips gives a field gradient to field ratio $(\partial H/\partial Z)/H$ at the beam position of 0.93 cm^{-1}. Each magnet coil has 2400 turns of No. 14 AWG copper wire and the coil forms are water cooled. Each magnet is supplied by its own transistorized regulated power supply which has a maximum output of 5 A.

The C-magnet system is the Varian V-4012A 12-in. electromagnet with the V-2100B regulated-magnet power supply. The pole-tip separation is 1.75 in. and the magnet is independent of the vacuum system.

There are two 1/2-× 3-× 12-in. hypernom plates in the vacuum tank between the C-magnet pole tips. These plates are separated by three quartz spacers and held together by brass clamps. The quartz spacers are 1/4 in. thick and have been ground to within 1/4 of a wave of each other. The radiofrequency hairpin slides into the 1/4-in. gap

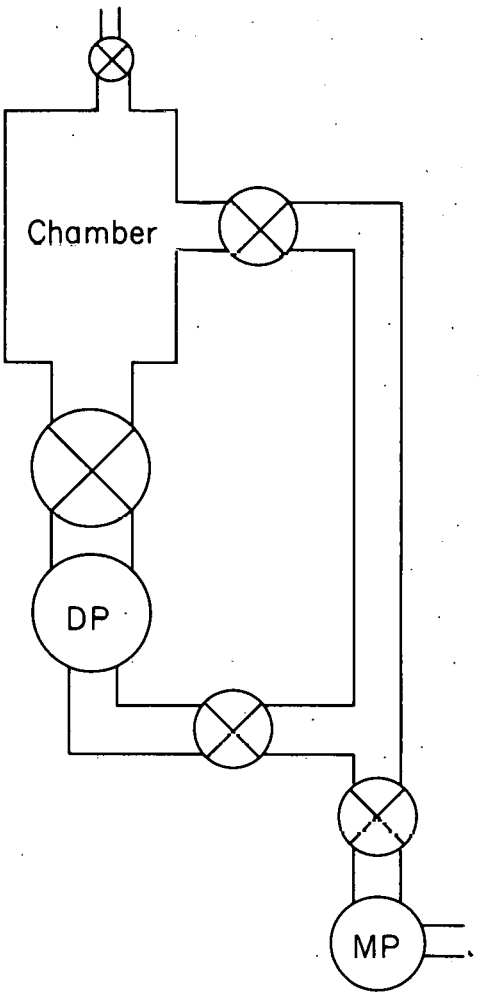

Fig. 7. Independent valve system for the oven and buffer chambers of atomic-beam machine B.

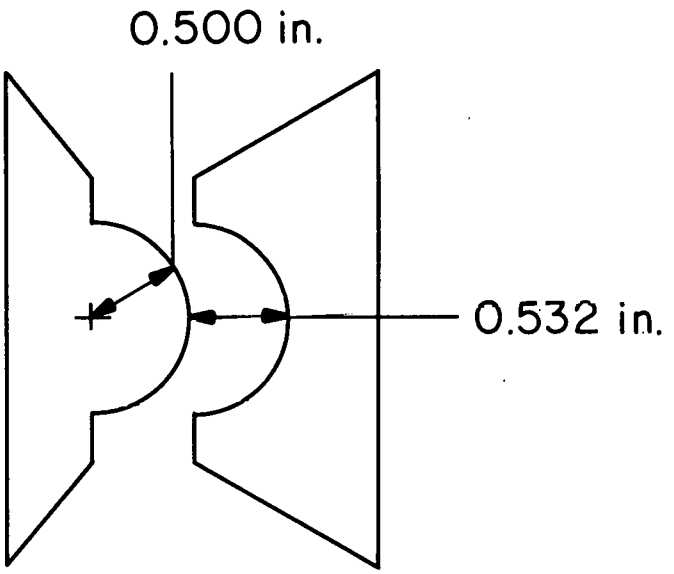

MU-32348

Fig. 8. Cross section of the A and B magnets of atomic-beam machine B.

between the hypernom plates. This system is shown in Fig. 9. By varying the position of the spacers and the pressure on the brass clamps, we could vary the homogeneity of the C field. The homogeneity thus obtained was about 3 parts in 10^5 over the 4 in. of the radio-frequency hairpin. With this magnet system, linewidths of 15 kc/sec were obtained with lithium and 2 kc/sec with cesium. A straight wire hairpin was placed next to the 4-in. hairpin to obtain broader lines. Its use was to assist in the initial search for resonances which were then narrowed down with the other hairpin. With this hairpin, a linewidth of 100 kc/sec was obtained with lithium.

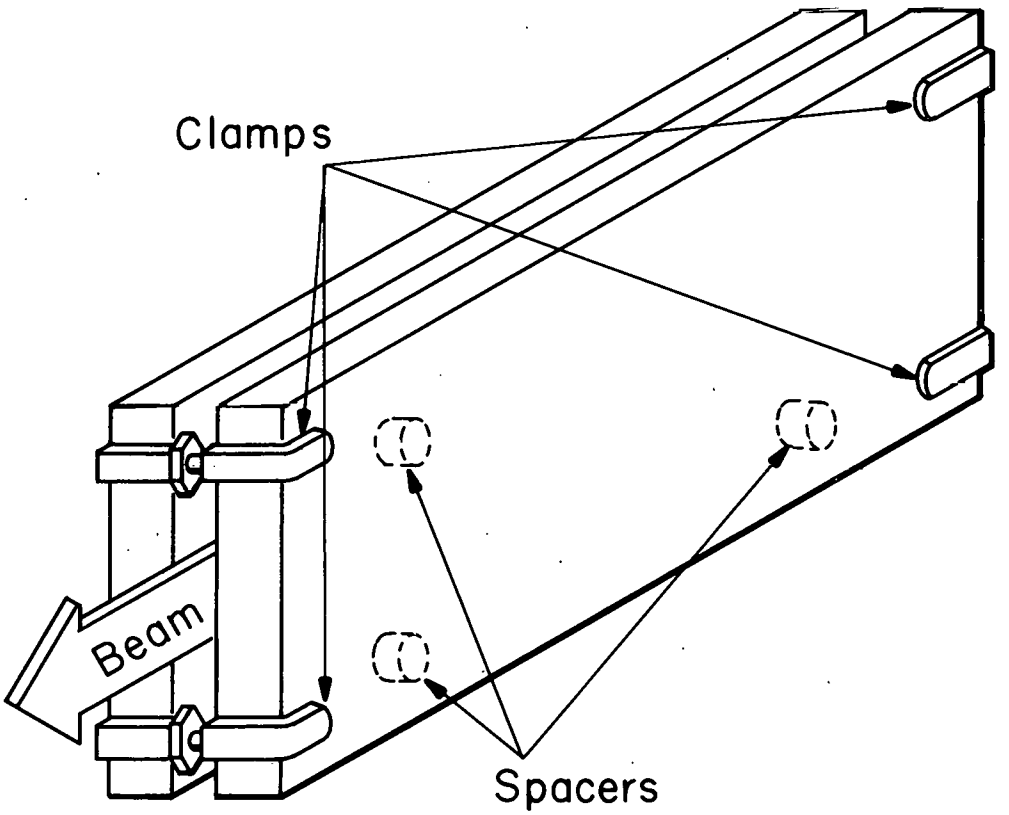

Fig. 9. C-magnet plate assembly for atomic-beam machine B.

V. THE LITHIUM EXPERIMENT

A. Introduction

The hyperfine-structure anomaly of hydrogen and deuterium and the lack of an anomaly between hydrogen and tritium have been well worked out theoretically.[24-26] Lithium is the next atom in the periodic table with an unpaired s electron. In 1949, Kusch and Mann[27] measured the hyperfine structure anomaly of Li^6 and Li^7, based on the hyperfine structure measurements of Kusch and Taub,[28] with this result,

$$_6\Delta_7 = +1.25(27) \times 10^{-4} .$$

The present experiment was done because we felt that nuclear wavefunctions of sufficient accuracy would soon be available to warrant an improvement in this value. The hyperfine-structure anomaly should be a good test of the validity of these wavefunctions.

Figures 10 and 11 give the Breit-Rabi diagrams [from Eq. (2.18)] of Li^6 and Li^7, respectively. The transitions that were observed are indicated. The Zeeman transition in Li^7, $(F = 2, m_F = -1) \longleftrightarrow (F = 2, m_F = -2)$, was used to calibrate the H_0 field. Observations were made on the $(F = 2, m_F = -1) \longleftrightarrow (F = 1, m_F = -1)$ transition in Li^7 and the $(F = 3/2, m_F = -1/2) \longleftrightarrow (F = 1/2, m_F = -1/2)$ transition in Li^6. The first excited level in lithium lies 14 904 cm^{-1} above the ground state. It could not be observed in the beam. Since all excited levels are so far removed from the ground state, the excited states produce a negligible effect on the purity of the ground state. Therefore, the assumption that both I and J are good quantum numbers is valid.

B. Beam Production and Detection

Lithium metal was loaded into a stainless steel oven of the type depicted in Fig. 12. The oven was then positioned on a three-pin platform which was connected to a high-voltage lead. Thoriated tungsten-filament wires were connected alongside the oven. This oven-loader arrangement was inserted into the oven chamber of atomic-beam machine B and the chamber was evacuated. A beam of

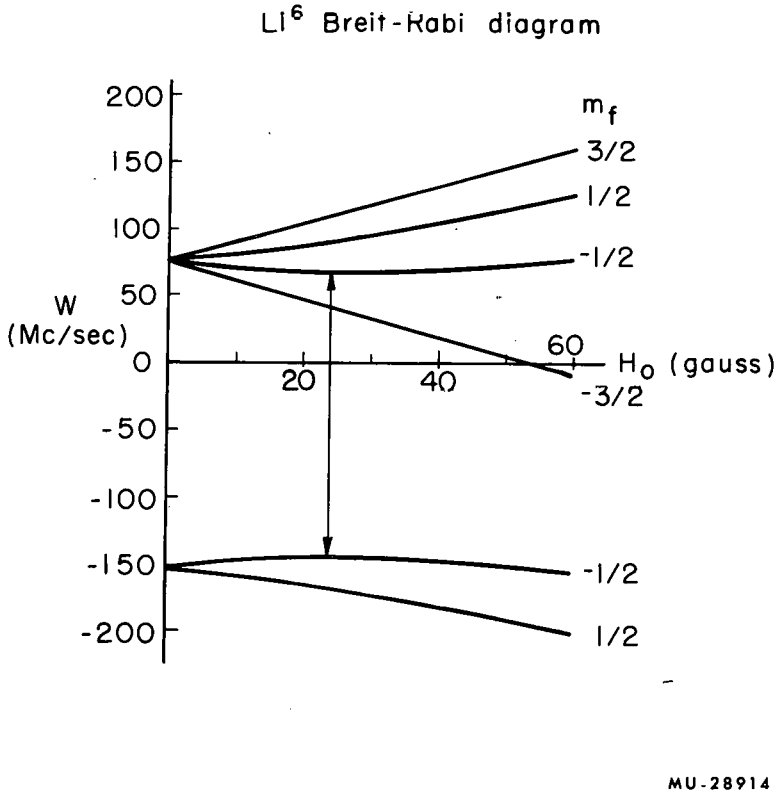

Fig. 10. Breit-Rabi diagram for Li^6.

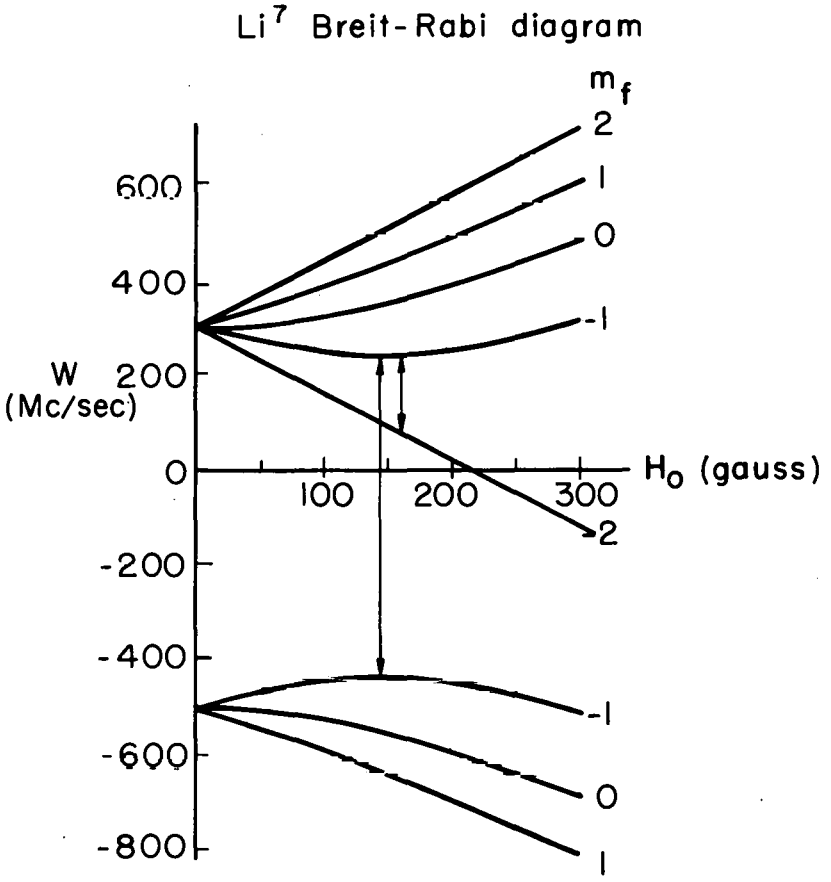

Fig. 11. Breit-Rabi diagram for Li^7.

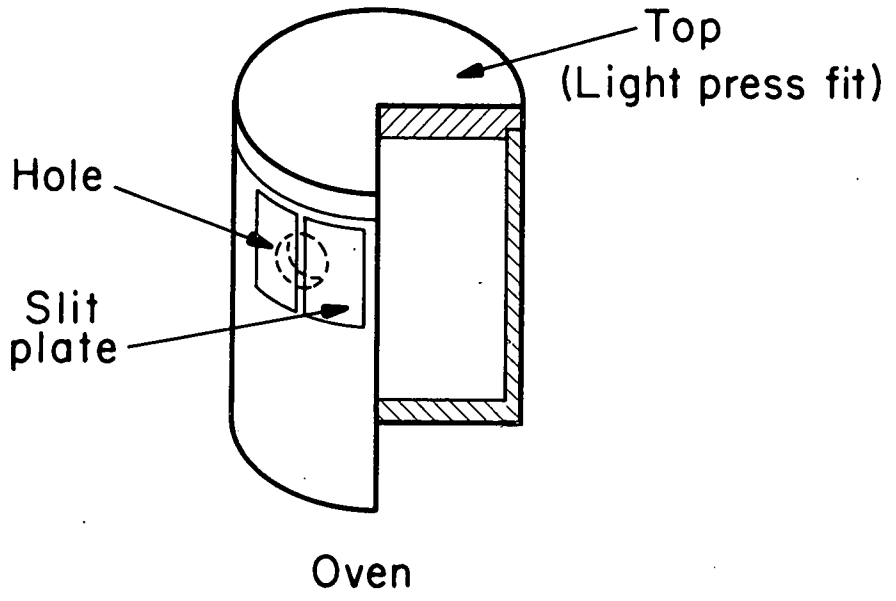

Fig. 12. Stainless steel oven used for the lithium experiment.

lithium atoms was produced by heating the stainless steel oven by electron bombardment. The oven had been given a positive potential with respect to the oven loader and sufficient current was passed through the thoriated tungsten filaments to obtain electron emission. The lithium atoms effused out of the oven through the 10-mil slits, as shown in Fig. 12.

The oven was then lined up by positioning the oven loader so as to maximize the output of the hotwire detector. A 100-mil iridium ribbon was used as a hotwire with approximately 8 A being fed through it. Oxygen at a pressure of 1×10^{-6} mm of mercury was bled into the detector chamber through a Vactronic bleeder valve and through a hypodermic needle pointed at the hotwire. The oxygen exhanced the detection efficiency of the iridium hotwire.

For the Li^7 hyperfine-structure determination the beam was chopped by a mechanical chopper that was driven by a 15-cps oscillator. The output of this oscillator and the signal from the hotwire were fed into a phase-sensitive detector. The output of the phase-sensitive detector was then observed on a Leeds and Northrup Speedomax recorder. A block diagram of the detection scheme is given in Fig. 13.

C. Radiofrequency System

The radiofrequency hairpin used is depicted in Fig. 14. It was situated between the two hypernom plates as described in Sec. IV-B-3. The hairpin was constructed of two 4×4-in. silver-plated copper plates. The beam passed along the face of one of the plates, and the constant H_0 field was perpendicular to both the beam and the hairpin. Two of the radiofrequency magnetic-field lines are shown. As the beam passed either edge of the copper plate it entered a region where the magnetic field of the radiofrequency signal was parallel to the constant H_0 field. The edges of the hairpin then gave rise to the separated oscillatory fields that are necessary to observe a Ramsey pattern.[29-31] A typical example of the types of patterns obtained is shown in Fig. 15.

Two radiofrequency oscillators were used in the course of the lithium experiment. A Rhode and Schwartz SLRD UHF Power Signal

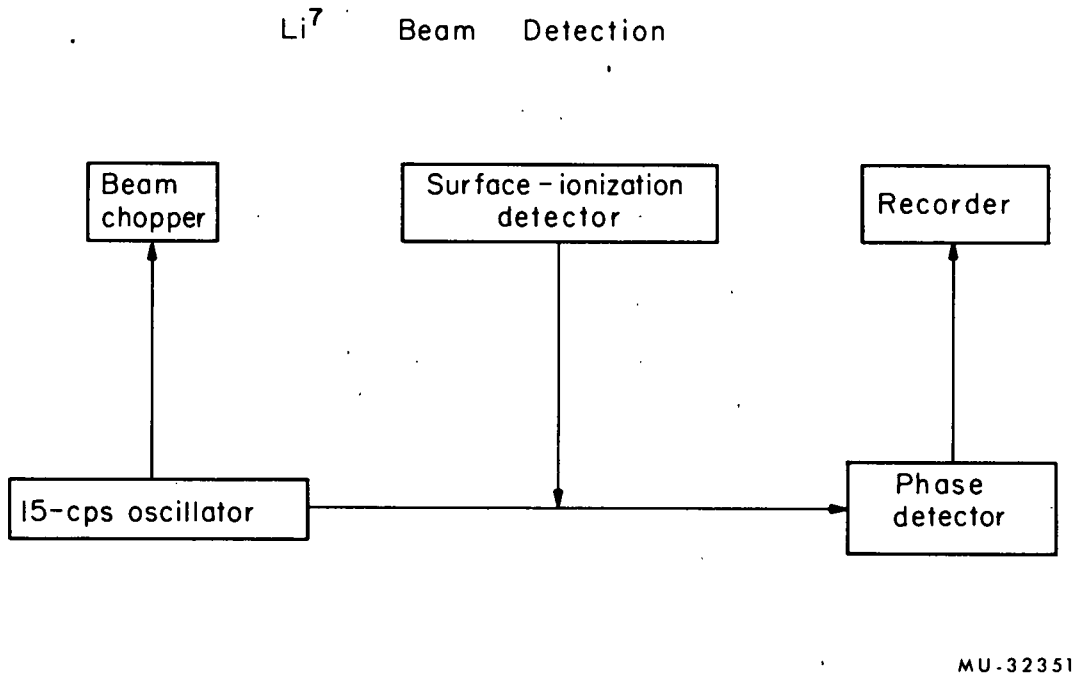

Fig. 13. Block diagram for the Li^7 detection system.

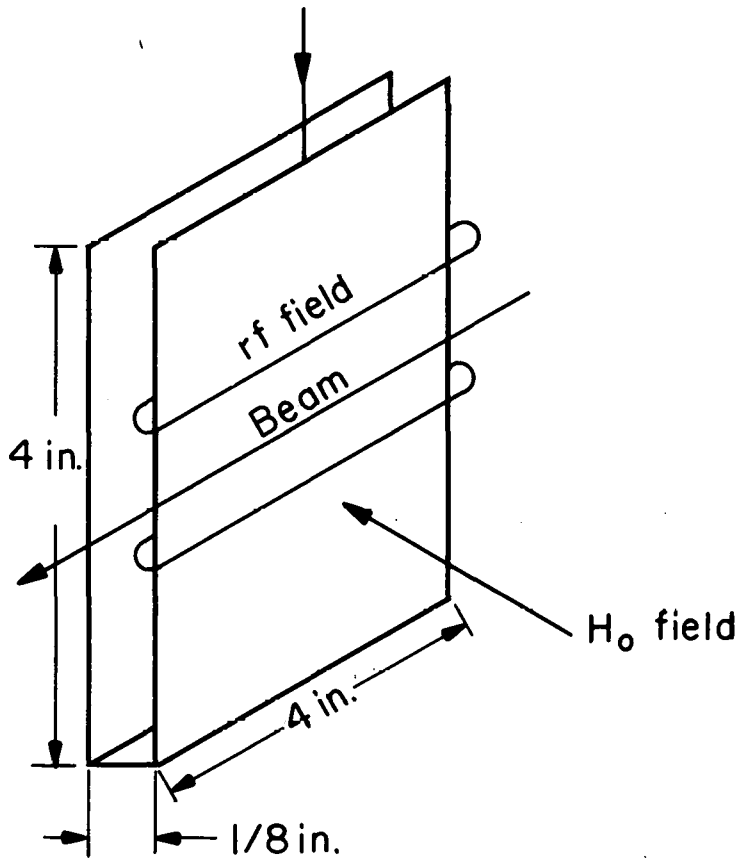

Fig. 14. Radiofrequency hairpin used for the lithium experiment.

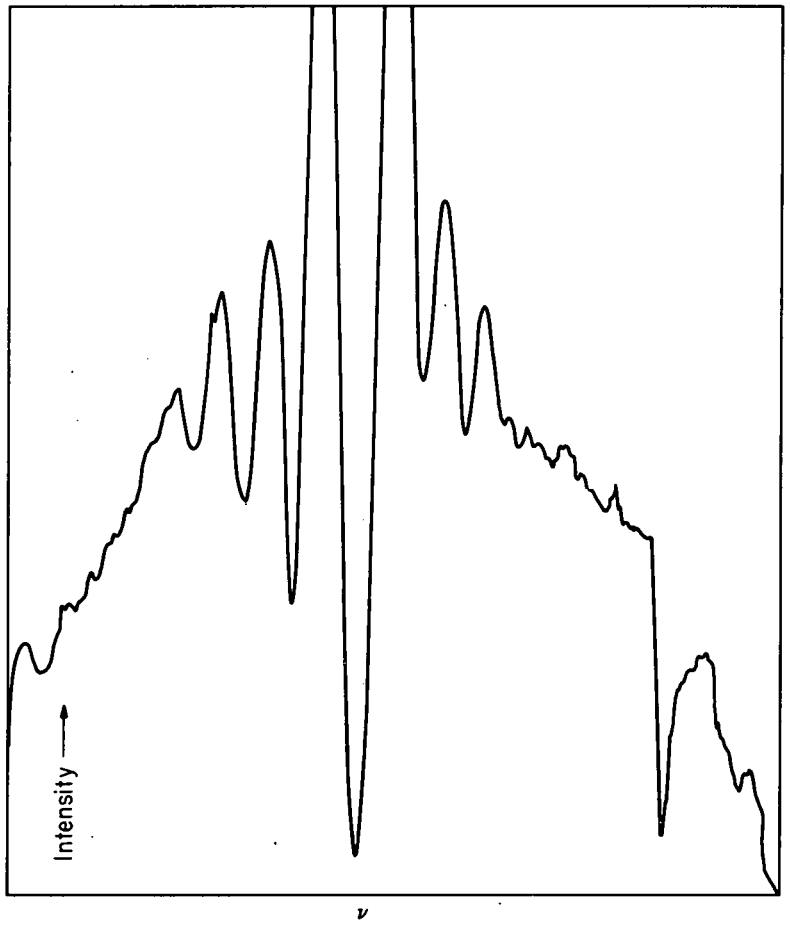

Fig. 15. Typical Ramsey pattern obtained with lithium--intensity vs frequency.

Generator was used for the $(F = 2, m_F = -1) \longleftrightarrow (F = 1, m_F = -1)$ transition in Li^7. A Hewlett-Packard model 540A Transfer Oscillator was used for both the Zeeman transition in Li^7 and the $(F = 3/2, m_F = -1/2) \longleftrightarrow (F = 1/2, m_F = -1/2)$ transition in Li^6. The signal from the transfer oscillator was amplified by an Instruments for Industry model-500 wideband amplifier. The frequency measurements were made with a Hewlett-Packard model-524C electronic counter with the model-525B and model-525C frequency-converter units. The oscillators were locked using the Schromandl FDS3 Syncriminator as a 10-Mc/sec phase-sensitive detector. A Manson model RD-140 1-Mc/sec crystal oscillator with the Manson model RD-125 100-kc/sec regenerative divider was used as the standard frequency. The standard was checked against the Atomicron and found to agree to within 2 parts in 10^7. The output of the frequency standard was multiplied to a value of 10 Mc/sec less than the output of the Rhode and Schwartz oscillator or the Hewlett-Packard transfer oscillator, whichever was being used. These two signals were fed into a mixer and the difference frequency was fed into the syncriminator. The syncriminator generated a correction voltage that was fed to the plate of the oscillator tube, hence locking the oscillator to the output of the multiplier. The 100-kc/sec output of the regenerative divider was also fed into the Hewlett-Packard electronic counter and the 10-Mc/sec output from the counter was fed to the x plate of an oscilloscope. The input to the y plate was the 10-Mc/sec input to the syncriminator. When the oscillator was locked to the output of the multiplier, a Lissajous figure was observed on the oscilloscope. If the input to the syncriminator does not have an appreciable amount of frequency modulation at a high frequency, we can say that the outputs of the oscillator and the frequency multiplier agree to within the rate of the turning over of the Lissajous figure.

For the Li^6 hyperfine-structure determination, the mechanical-beam chopping technique was not used. Instead the radiofrequency signal was modulated at 15 cps with the General Radio type 1000-P7 balanced modulator. This increased the signal-to-noise ratio for the less abundant isotope.

In Fig. 16 is shown the radiofrequency and locking equipment that was used in the lithium experiment. A block diagram of the radiofrequency system is given in Fig. 17. More detailed block diagrams of the radiofrequency systems for the Li^6 and Li^7 hyperfine-structure determinations are given in Figs. 18 and 19, respectively.

D. Results

For the transition frequency between two hyperfine-structure levels of an atom with $J = 1/2$ we have

$$\nu = W_{I+\frac{1}{2}} - W_{I-\frac{1}{2}} . \tag{5.1}$$

From Eq. (2.18) we see that for the observed direct transition in Li^6 and Li^7 we can write

$$\nu = \Delta\nu[1 - 2(2I - 1)/(2I + 1)\, x + x^2]^{\frac{1}{2}} . \tag{5.2}$$

Taking the first derivative, we obtain

$$\begin{aligned} \partial\nu/\partial x &= \Delta\nu/2 \; \frac{2x - 2(2I - 1)/(2I + 1)}{[1 - 2(2I - 1)/(2I + 1)\, x + x^2]^{\frac{1}{2}}} \\ &= (\Delta\nu)^2/\nu \; [x - (2I - 1)/(2I + 1)] . \end{aligned} \tag{5.3}$$

We see that the transition frequency reaches a minimum at a value of x (i. e., of H_0) of

$$x_{min} = (2I - 1)/(2I + 1) . \tag{5.4}$$

Taking the second derivative, we obtain

$$\partial^2\nu/\partial x^2 = \Delta\nu \left\{ [1 - 2(2I - 1)/(2I + 1)\, x + x^2]^{-\frac{1}{2}} - \frac{[x - (2I - 1)/(2I + 1)]^2}{[1 - 2(2I - 1)/(2I + 1)\, x + x^2]^{3/2}} \right\} ,$$

$$\partial^2\nu/\partial x^2 = (\Delta\nu)^2/\nu - [(\Delta\nu)^4/\nu^3] \; [x - (2I - 1)/(2I + 1)]^2 . \tag{5.5}$$

By expanding the transition frequency in a Taylor's series about the minimum transition frequency, we obtain

$$\nu \approx \nu_{min} + [(\Delta\nu)^2/2\nu_{min}] \; (x - x_{min})^2 . \tag{5.6}$$

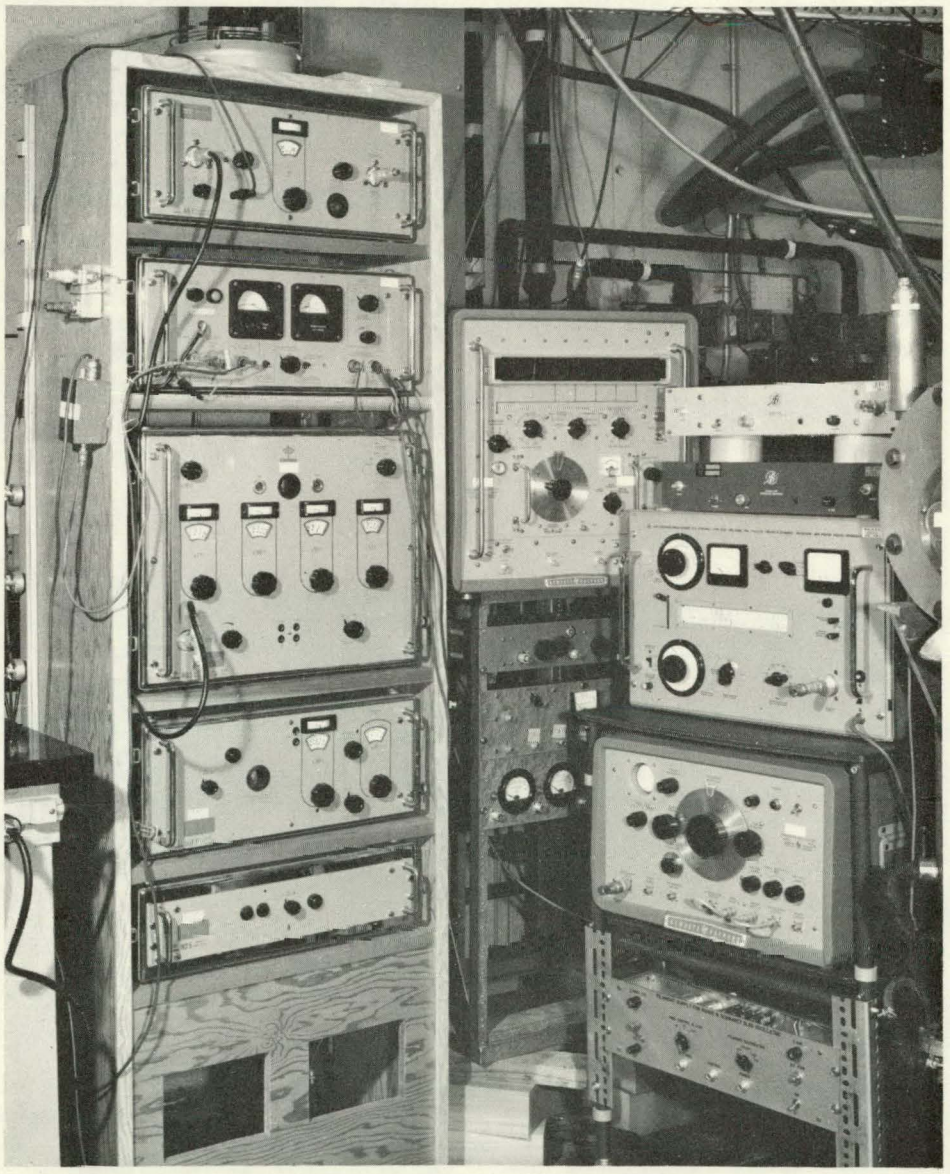

ZN-4007

Fig. 16. Radiofrequency and locking equipment used during the lithium experiment.

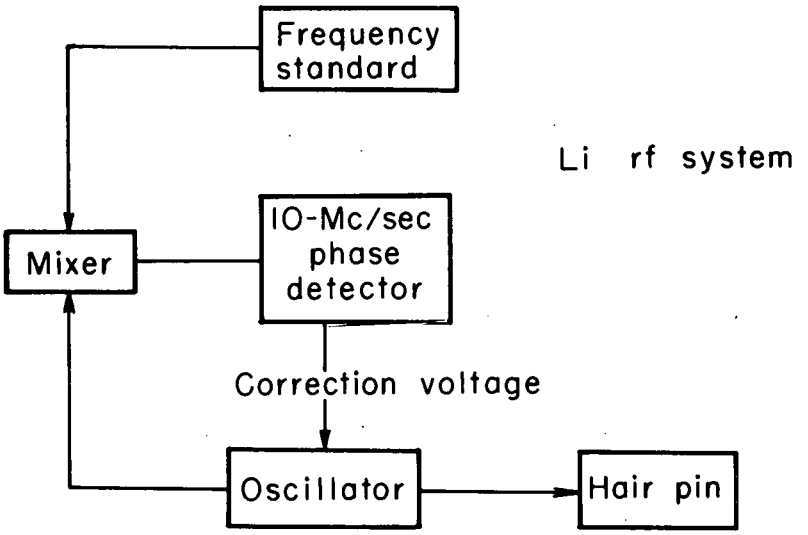

Fig. 17. Block diagram of the lithium radiofrequency system.

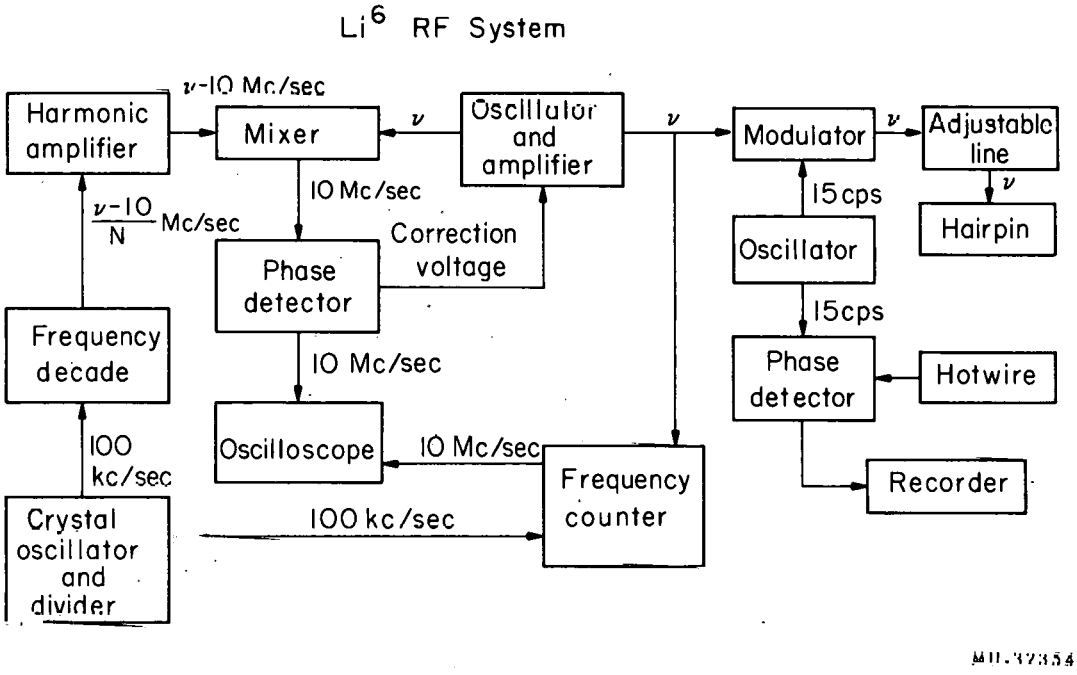

Fig. 18. Detailed block diagram of the radiofrequency system used for the Li^6 hyperfine-structure determination.

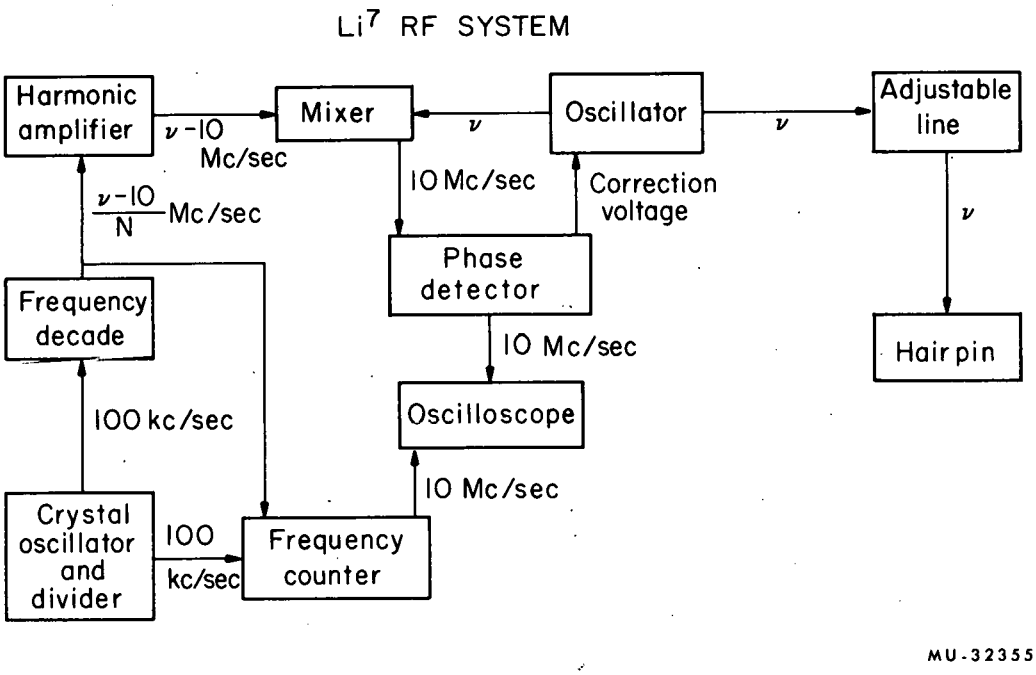

Fig. 19. Detailed block diagram of the radiofrequency system used for the Li^7 hyperfine-structure determination.

From Eq. (5.2) we see that ν_{min} is related to the hyperfine-structure separation by

$$\Delta\nu = \nu_{min}\left\{1 - [(2I-1)/(2I+1)]^2\right\}^{-\frac{1}{2}} \qquad (5.7)$$

Therefore, we have

$$\nu \approx \nu_{min}\left\{1 + [(2I+1)^2/16I](x - x_{min})^2\right\} . \qquad (5.8)$$

Therefore, by making a least-squares fit of the observed transition frequencies in the neighborhood of the minimum transition frequency to the above parabola, we obtain the best value for ν_{min}. From Eq. (5.7) we then obtain the hyperfine-structure separation. This scheme has the advantage of not being dependent on the field error to first order.

The experimental data that was obtained on the Li^7 direct transition is given in Table III. Two sets of data were obtained on this transition, each set being taken for a different orientation of the radio-frequency hairpin. This was done to determine how much the phase difference between the separated oscillating fields was shifting the lines. It proved to be on the order of 120 cps, which was of the same order as the frequency errors. The experimental data that was obtained on the Li^6 direct transition is given in Table IV. The data for both isotopes is plotted in Fig. 20, and the curves shown there are the least-squares fit to the data obtained.

For the results we thus obtained for Li^6

$$\nu_{min} = 215.15400(8) \text{ Mc/sec} ,$$

and, therefore,

$$\Delta\nu_6 = 228.20528(8) \text{ Mc/sec} .$$

For Li^7 we obtained

$$\nu_{min} = 695.85491(40) \text{ Mc/sec},$$

and, therefore,

$$\Delta\nu_7 = 803.50404(48) \text{ Mc/sec} .$$

Table III. Experimental data for Li^7.

First orientation		
Run	$\nu(F = 2, m_F = -1) \longleftrightarrow (F = 1, m_F = -1)$	ν_z (in Li^7)
1	695.85524(10)	147.091 (6)
2	695.85488(10)	146.746(12)
3	695.85530(10)	146.499 (6)
4	695.85503(10)	146.636 (6)
5	695.85500(10)	146.888 (6)
Second orientation		
Run	$\nu(F = 2, m_F = -1) \longleftrightarrow (F = 1, m_F = -1)$	ν_z (in Li^7)
1	695.85473(12)	146.739 (3)
2	695.85494(12)	146.909 (3)
3	695.85512(12)	146.510 (4)
4	695.85497(12)	146.633 (4)
5	695.85485(12)	146.803 (3)

Table IV. Experimental data for Li^6

Run	$\nu(F = 3/2, m_F = -1/2) \longleftrightarrow (F = 1/2, m_F = -1/2)$	ν_z (in Li^7)
1	215.15420(12)	20.300(3)
2	215.15425(21)	20.259(2)
3	215.15420 (9)	20.324(2)
4	215.15432 (5)	20.492(3)
5	215.15406 (6)	20.403(2)
6	215.15458 (4)	20.246(2)
7	215.15410 (3)	20.456(2)
8	215.15406 (7)	20.359(2)

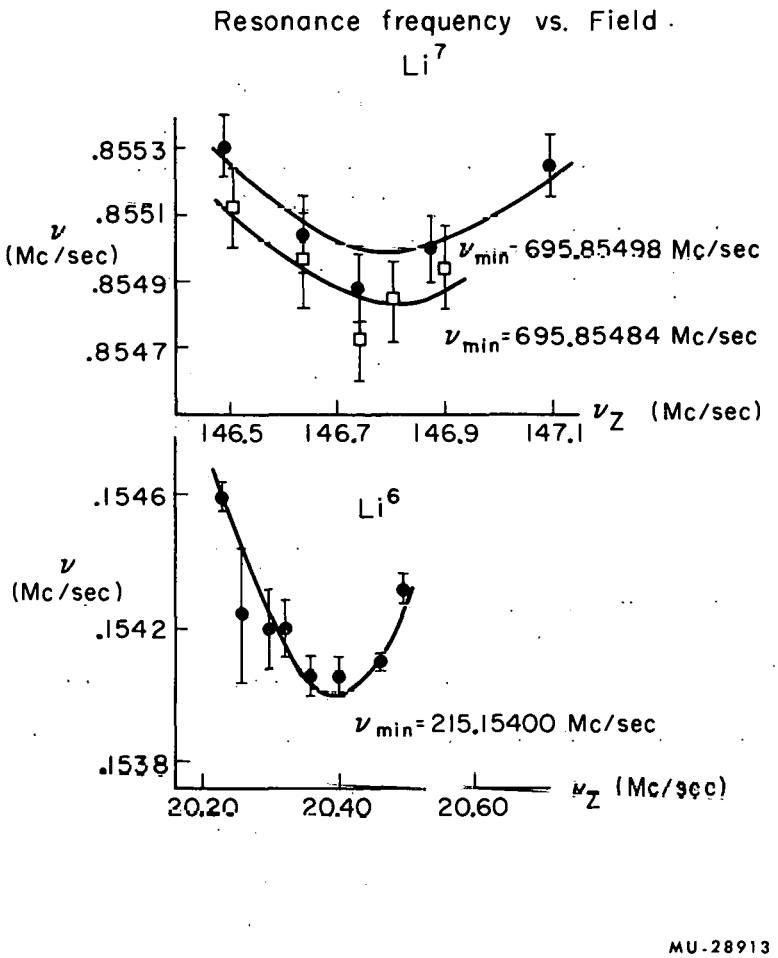

Fig. 20. Li^6 and Li^7 data plots and the corresponding least squares fit curves.

The errors quoted are four times the statistical errors.

From Eqs. (2.26) and (2.29) we obtain for the hyperfine-structure anomaly between the isotopes Li^6 and Li^7 the expression

$$ {}_6\Delta_7 = 1 - \frac{\Delta\nu_7 \, g_{I_6}}{\Delta\nu_6 \, g_{I_7}} \left(\frac{2I_6+1}{2I_7+1}\right) \left(\frac{\mu_6}{\mu_7}\right)^3 . \qquad (5.9) $$

Using the ratio of the g_I values as obtained by Klein,[32]

$$ g_{I_7}/g_{I_6} = 2.64090588(20) , $$

we obtain for the hyperfine-structure anomaly of the isotopes Li^6 and Li^7 the value

$$ {}_6\Delta_7 = +1.065(6) \times 10^{-4} , $$

where the quoted error is four times the statistical error.

VI. THE RHENIUM EXPERIMENT

A. Introduction

In the past, the high melting points and low vapor pressures of the refractory elements (atomic numbers 71 through 78) have made it difficult to obtain atomic beams of sufficient intensity for study. Recently, Doyle has been successful in producing such beams and has determined the nuclear spins of many of the refractory isotopes.[33]

In 1931, Meggers[34] made optical spectroscopy studies of the electronic properties of rhenium. He determined the g_J factor but with relatively poor accuracy. The validity of Russell-Saunders coupling and the relativistic and diamagnetic shielding corrections to it could be tested if there were an improved value of g_J.

Since rhenium lies in a region of high nuclear deformation, its nuclear properties should be a good test of the collective model of the nucleus, which is discussed at length by other authors.[35-39]

B. Experimental Method

The usual method of beam production by heating a substance in an oven was not feasible for rhenium. Virtually any oven material would melt before sufficient beam intensity could be attained or would react with the rhenium. Instead, the method of heating a rhenium wire by electron bombardment was used.

The isotopes Re^{186} and Re^{188} were produced by bombarding a 3/4-in. piece of 20-mil natural rhenium wire in the General Electric Test Reactor at the Vallecitos Atomic Laboratory in Pleasanton, California. The neutron flux was 1×10^{14} neutrons/cm^2/sec. The 100-mg samples were then transported to the Lawrence Radiation Laboratory. Rhenium-185 has an abundance of 37.07% and a cross section for neutron capture of 110 barns. For the production of the Re^{186} isotope, the samples were irradiated for 72 hours and then decayed for five to nine days. Therefore, at least 2.9 curies of Re^{186} were present in the samples. The amount of Re^{188} activity in the beam was less than 5%, as shown by decay plots of samples of both the full beam and resonances. The Re^{186} and Re^{188} have half lives of

90 hours and 17 hours, respectively. Therefore, their existence could easily be discerned in such a decay plot. Rhenium-187 has an abundance of 62.93% and a cross section for neutron capture of 70 barns. Rhenium-188 was preferentially produced by bombarding the samples for 3 to 4 hours. This yielded 4 to 6 curies of Re^{188} and approximately 20% as much activity of Re^{186}. This was confirmed and resonances identified by decay plots.

Upon receipt of the radioactive sample we placed it in a lead-shielded "cave" as shown in Fig. 21. With the use of manipulators the wire was positioned in the oven loader. The oven loader is shown in Fig. 22. The rhenium wire was placed into the 20-mil hole drilled into the tantalum post shown in the center of the picture. The post fitted into the tantalum mounting piece, which was firmly fixed to the high-voltage lead shown in the center of the oven loader assembly on the left. The tantalum ground shield to the right of the oven-loader assembly rested on the water cooling pipes. The rhenium wire protruded up through the 1/4-in. hole in the ground shield. The purpose of the ground shield was to protect the high-voltage leads from excessive heating due to electron bombardment. Thoriated tungsten filament wires were attached to the two sets of mounting posts in the oven-loader assembly. These posts can be seen in line with the water cooling pipes. The part on the far right of the picture is the lid for the oven-loader assembly. Sufficient current to produce electron emission was passed through the filament wires. A positive voltage was then applied to the wire, which was heated by electron bombardment. This scheme has worked well and beams of sufficient intensity and stability for the experiment have lasted from 5 to 10 hours.

The wire could easily be lined up in the machine by placing enough voltage on the wire to make it glow and then optically lining the wire up with the slits. The edges of the wire could be distinguished at the detector end of the machine with the aid of a small hand telescope.

When the wire had been heated to a high enough temperature to produce a beam, the atoms were collected on 1-mil fired platinum foils, which were slid into a holder. The holder is shown on the left

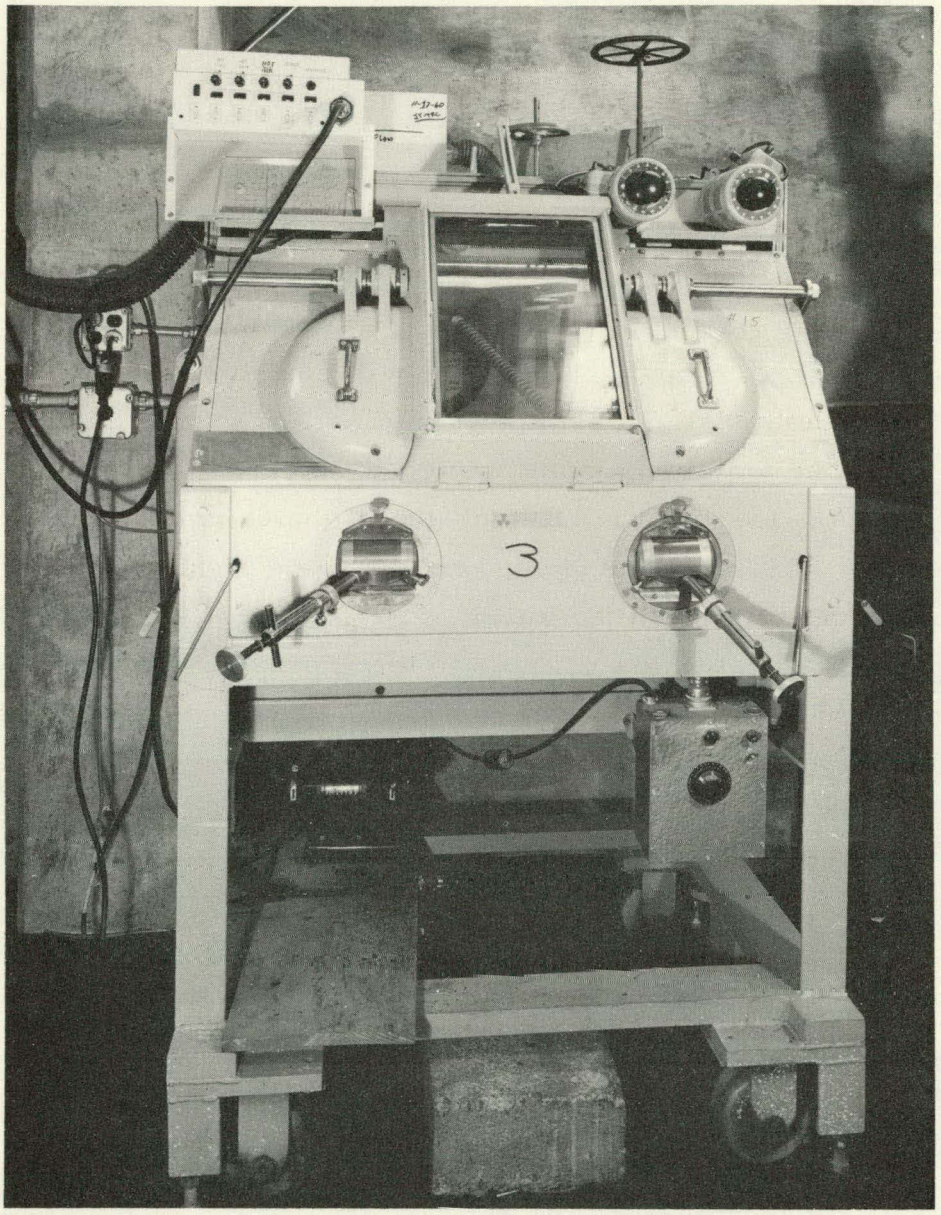

ZN-2677

Fig. 21. Lead-shielded "cave" for handling radioactive materials.

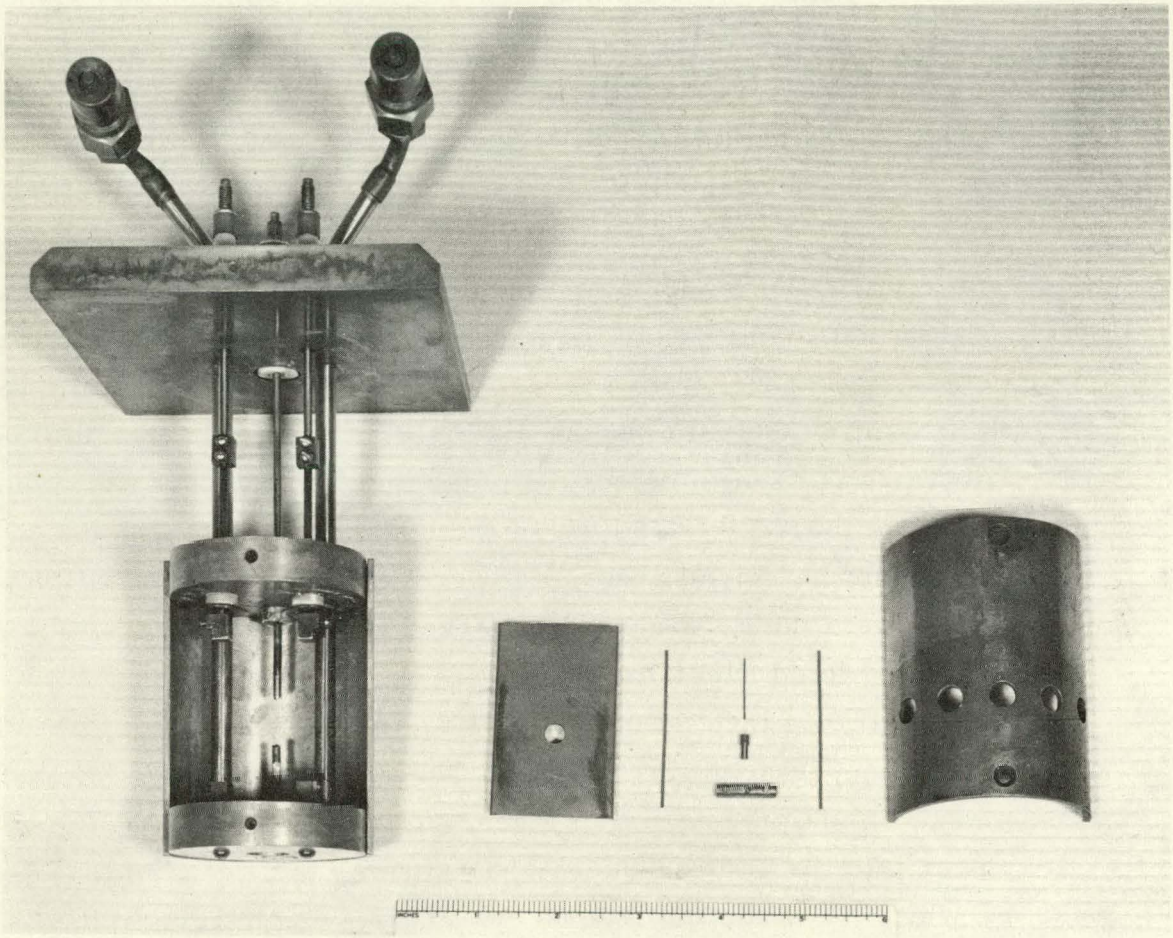

ZN-4006

Fig. 22. Oven-loader assembly used for the rhenium experiment.

of Fig. 23. The holder is locked into position in a plate that can be rotated into the beam position and then, after exposure, rotated out again and the foil removed. The button-loader assembly is shown in Fig. 24. A more complete description of this arrangement has been given by Brink.[40] (This button-loader arrangement was also built into atomic-beam machine B.) The foils were then placed in continuous-flow methane beta counters and the collected activity counted. The counters are shown in Fig. 25 and a drawing of the counting head assembly is shown in Fig. 26. These counters have been fully described elsewhere.[41] A full-beam counting rate of from 600 to 1200 counts per min after a 1-min exposure was determined to be the most convenient.

A calibration oven located in the buffer chamber was loaded with potassium. The Zeeman transition frequency in potassium was used to determine the value of the H_0 field. A 100-mil rhenium-ribbon hotwire was used to detect the potassium beam. The hotwire could easily be moved into and out of the beam position. The calibration oven could be raised and then lowered into the beam position. The signal from the hotwire was observed by the Applied Physics model-31 Vibrating Reed Electrometer.

A list of the radiofrequency equipment used during the rhenium experiment is given in Table V. The frequency ranges of each of these pieces of equipment is also given. The means of determining the power into the radiofrequency hairpin was the same as that described by White.[23] Since the frequency errors, which were in the neighborhood of 1 kc/sec, were a small fraction of the reasonance linewidths, which were 40 to 50 kc/sec, they were neglected.

C. Results

Theoretically, rhenium should have no hyperfine structure, since its electronic ground state is $^6S_{5/2}$. This is shown classically in the appendix. However, due to the breakup of Russell-Saunders coupling and the effects of configuration interaction, this is not the case. Other examples of this are given in the papers of Marrus, Nierenberg, and Winocur,[42] and Sandars and Woodgate.[43]

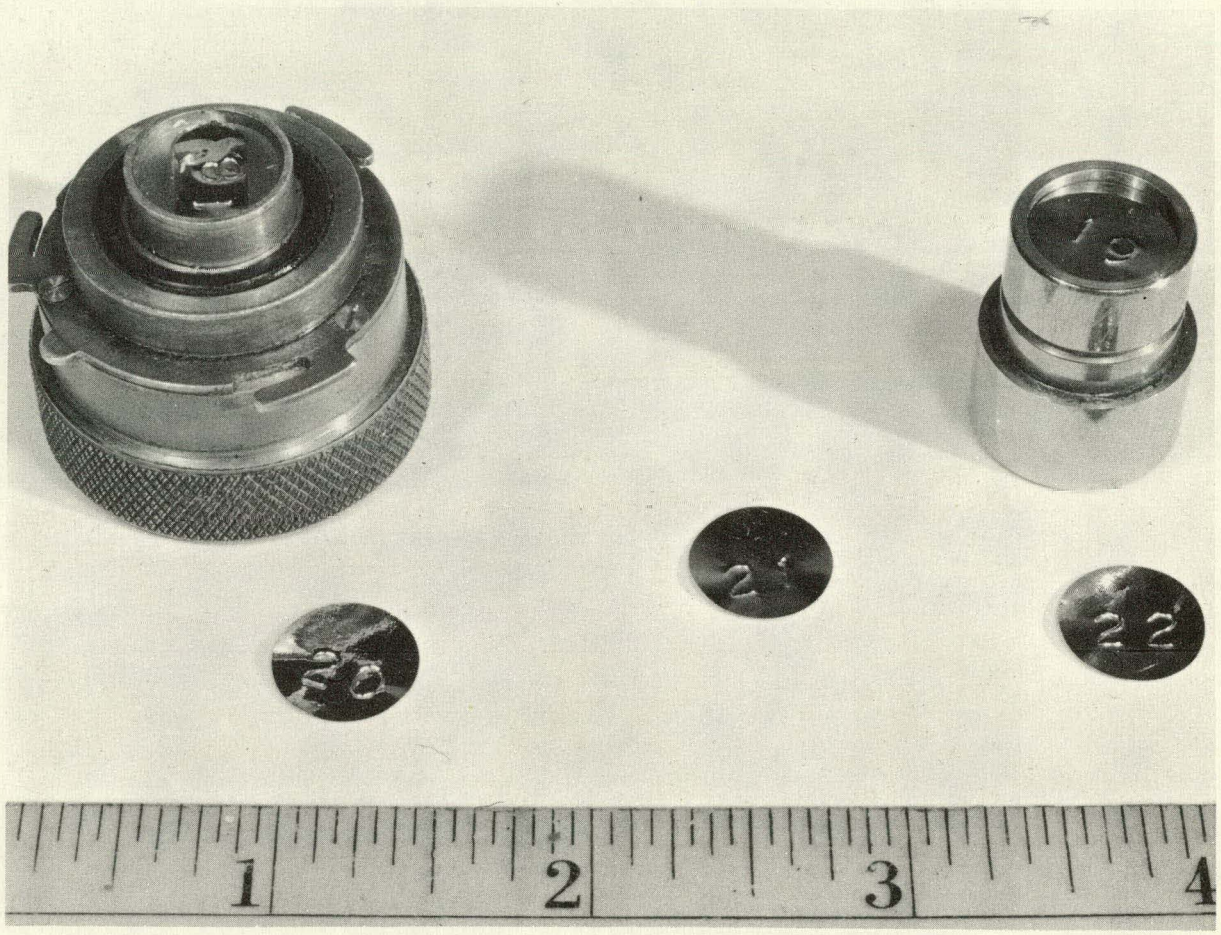

ZN-2936

Fig. 23. Foil holder, foils, and β-counter holder used for the detection of the rhenium beam.

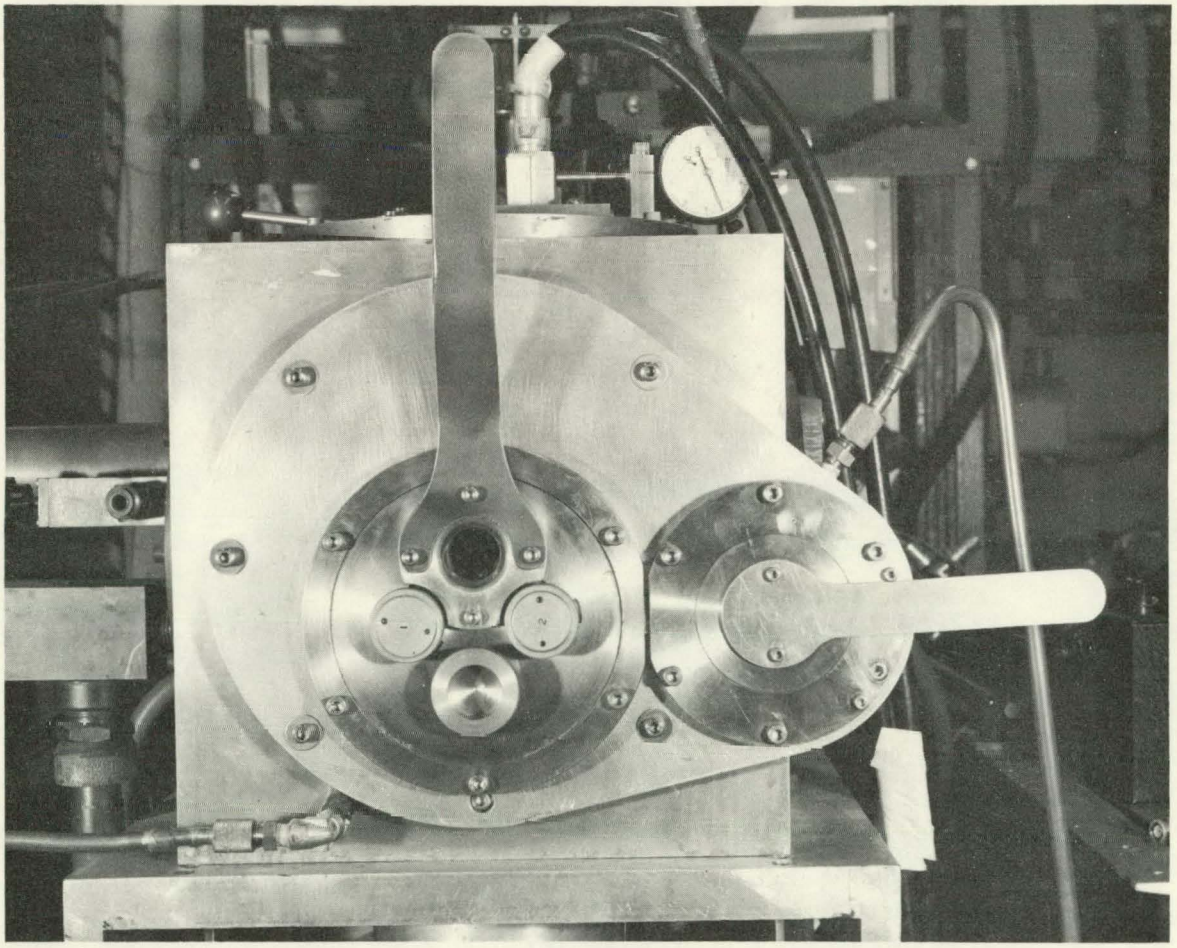

ZN-4009

Fig. 24. Button-loader assembly of atomic-beam machine A.

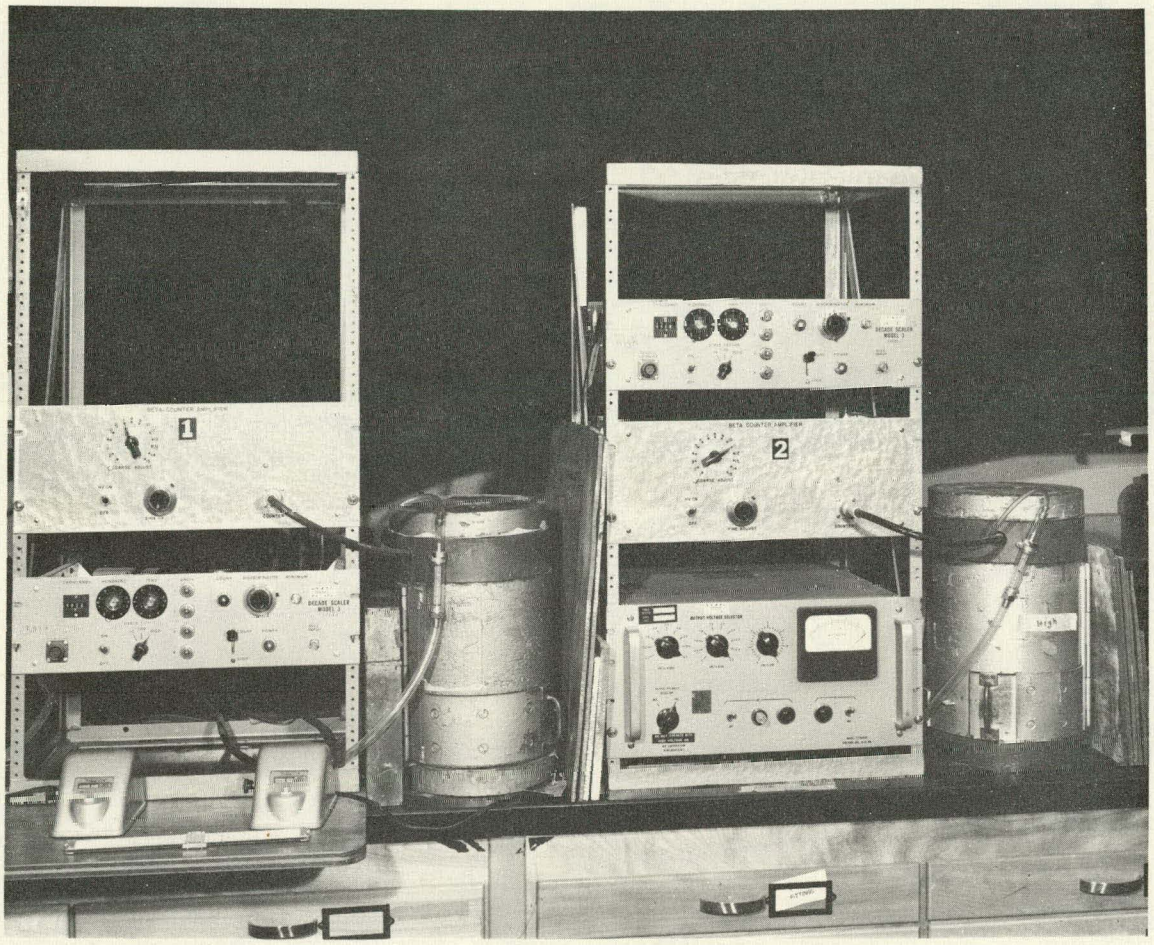

ZN-4008

Fig. 25. Proportional β counters used for the rhenium experiment.

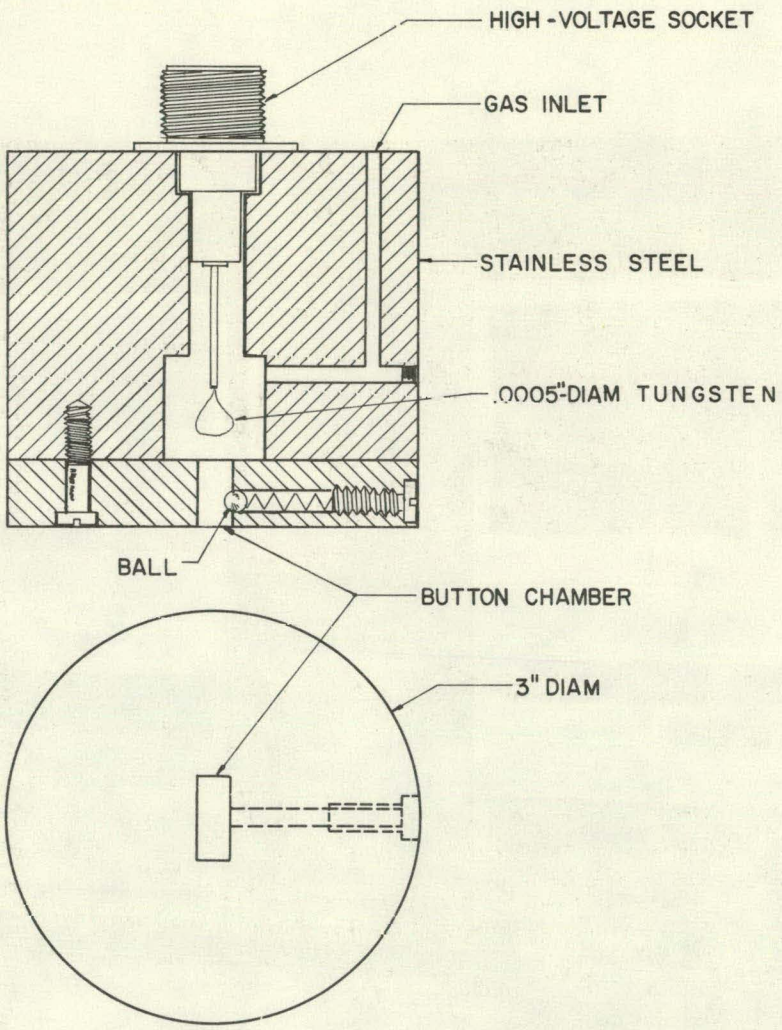

Fig. 26. Schematic cross section of the β-counter head assembly.

Table V. Radiofrequency equipment used for the rhenium experiment.

Radiofrequency equipment	Frequency range (Mc/sec)
Oscillators:	
General Radio type 805-C signal generator	0.016–50.0
Tektronix type 190A signal generator	0.35–50.0
Hewlett-Packard model 608A signal generator	10.0–500.0
General Radio type 1209B unit oscillator	250.0–920.0
Hewlett-Packard model 540A transfer oscillator	100.0–220.0
Amplifiers:	
IFI model 500 wide-band amplifier	0.5–240.0
IFI model 510 wide-band amplifier	0.5–240.0
Frequency Measuring Instruments:	
Hewlett-Packard model 524B electronic counter	
Hewlett-Packard model 525A frequency converter unit	0.0–100.0
Hewlett-Packard model 525B frequency converter unit	100.0–220.0
Hewlett-Packard model 525C frequency converter unit	100.0–500.0
Auxiliary Equipment:	
Simpson model 37 radiofrequency galvanometer	
Weston model 301 dc microammeter	
General Radio model 874 adjustable line	
General Radio model 874-LBA slotted line	
General Radio model 874-D50 50-cm adjustable stub	

The nuclear spin of both Re^{186} and Re^{188} has been measured by Doyle and Marrus to be 1 in both isotopes.[44] The resulting hyperfine-structure energy-level diagram for these two isotopes of rhenium is shown in Fig. 27. The observed transitions are also indicated. From Eq. (2.15) we see that in the low field approximation the transition frequency for the α, β, and γ transitions is given by

$$\nu = -g_F \mu_0 H_0 . \tag{6.1}$$

Neglecting the nuclear term we have the so-called Zeeman transition frequency

$$\nu = -g_J \frac{F(F+1) + J(J+1) - I(I+1)}{2F(F+1)} \mu_0 H_0 . \tag{6.2}$$

We first observed the α, β, and γ transitions at low field by using Eq. (6.2) to predict the transition frequency. These three transitions were then followed up in field until they started to diverge from the Zeeman frequency. Since it was predicted that rhenium would have a small hyperfine structure, deviations from the Zeeman frequency should occur at relatively small fields. Deviations from the predicted frequency were first seen at about 10 G. A third-order perturbation procedure given by White[23] was then used to predict the transition frequencies at higher fields. When enough points had been observed, we used the "HYPERFINE-3" computer program (written by Nierenberg and discussed elsewhere[45-47]) to determine initial values of the magnetic-dipole interaction constant, a, and the electric-quadrupole interaction constant, b. The JO-9 computer program[47] was then used to predict the transition frequencies at even higher fields, using the a and b values as calculated by HYPERFINE-3. In this manner, the α, β, and γ transitions were observed at fields as high as 200 G. At this point it was felt that the values of a and b were known with sufficient accuracy to begin searching for the direct transitions $(F = 7/2,\ m_F = -1/2) \longleftrightarrow (F = 5/2,\ m_F = -1/2)$ and $(F = 5/2,\ m_F = 1/2) \longleftrightarrow (F = 3/2,\ m_F = 1/2)$. Note that both direct transitions are σ transitions ($\Delta m_F = 0$). The π hairpin that was used to observe the α, β, and γ transitions was also used to observe the

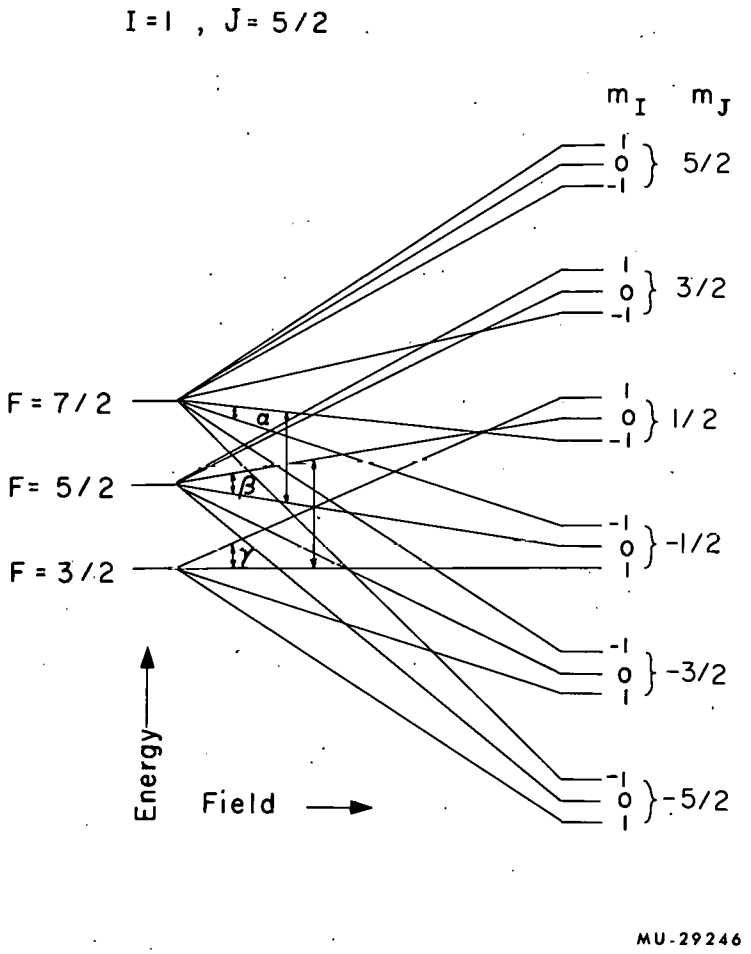

Fig. 27. Breit-Rabi diagram for Re^{186} and Re^{188}.

direct transitions. This hairpin consisted of a strip of metal, so the same situation existed as that described previously for the σ transitions of the lithium experiment. In this way, Ramsey patterns were also observed for both direct transitions in rhenium. It was determined by the JO-9 computer program that the transition $(F = 5/2,\ m_F = 1/2) \longleftrightarrow (F = 3/2,\ m_F = 1/2)$ attained a minimum transition frequency at approximately 12 G. Both direct transitions were observed at this field for each isotope. Representative resonances which were obtained are shown in Figs. 28 through 35, the direct transitions showing a dip rather than a peak at the transition frequency.

Tables VI and VII give the final HYPERFINE-3 output for the isotopes Re^{186} and Re^{188}, respectively. A measure of the goodness of the fit of the experimental points to the theoretical predictions using the a and b values obtained is the value of the goodness-of-fit parameter χ^2. Theoretically χ^2 should have the value N - N', where N is the number of observations and N' is the number of variables.[48] This predicts values of 6 and 5 for χ^2 for the Re^{188} and Re^{186} data, respectively. The values of 0.4 and 1.3, which were obtained by HYPERFINE-3 for Re^{188} and Re^{186}, respectively, indicate that pessimistic values of the frequency errors were used. Thus, the frequency errors as given by the HYPERFINE-3 program are also pessimistic. However, for security, twice these values will be used as the experimental errors. Therefore for the results we obtain, for Re^{186}, the values

$$a = \pm 78.3058(24) \text{ Mc/sec},$$

$$b = \mp\ 8.3601(50) \text{ Mc/sec},$$

and

$$g_I > 0 .$$

For Re^{188} we obtain the values

$$a = \pm 80.4320(32) \text{ Mc/sec},$$

$$b = \mp\ 7.7455(60) \text{ Mc/sec},$$

and

$$g_I > 0 .$$

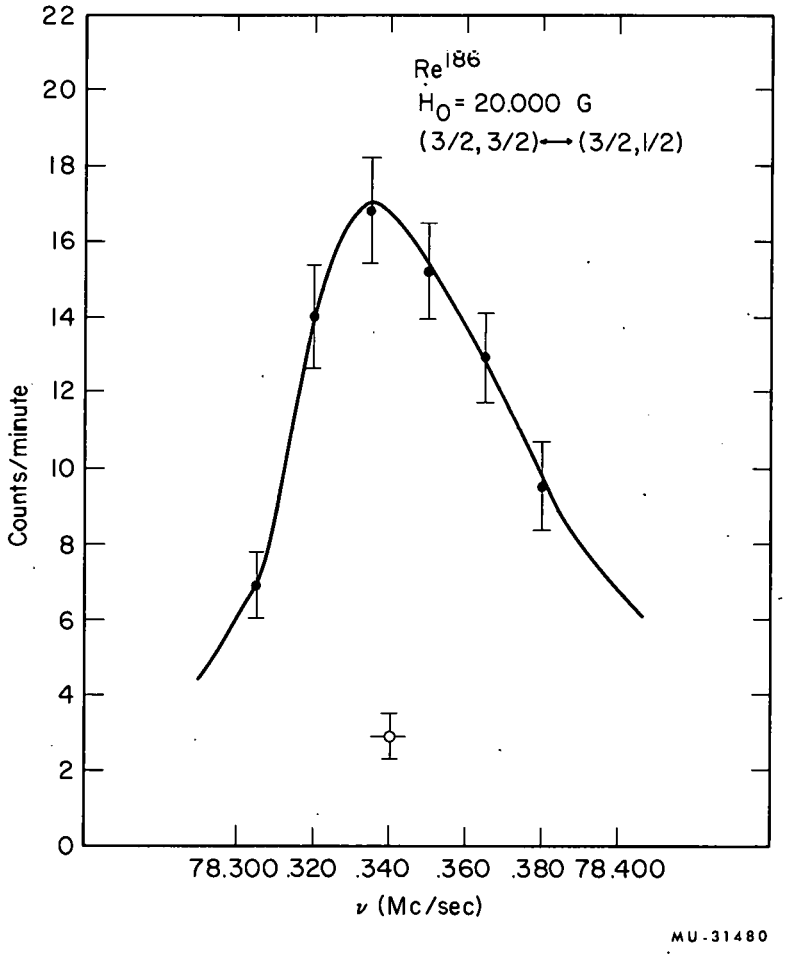

Fig. 28. Gamma transition in Re^{186} at 20.000 G.

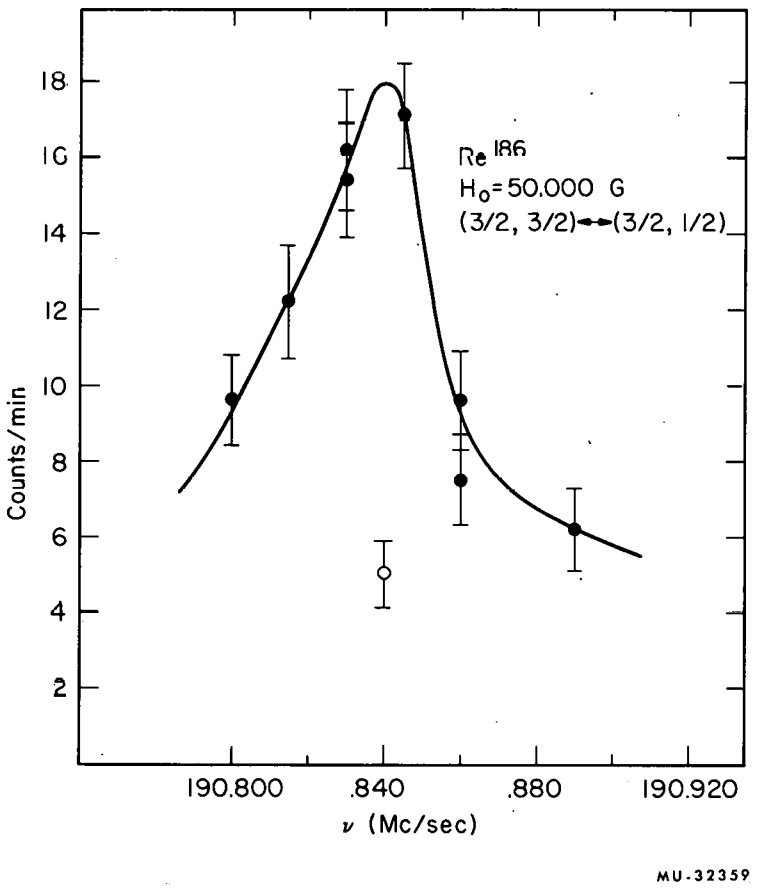

Fig. 29. Gamma transition in Re^{186} at 50.000 G.

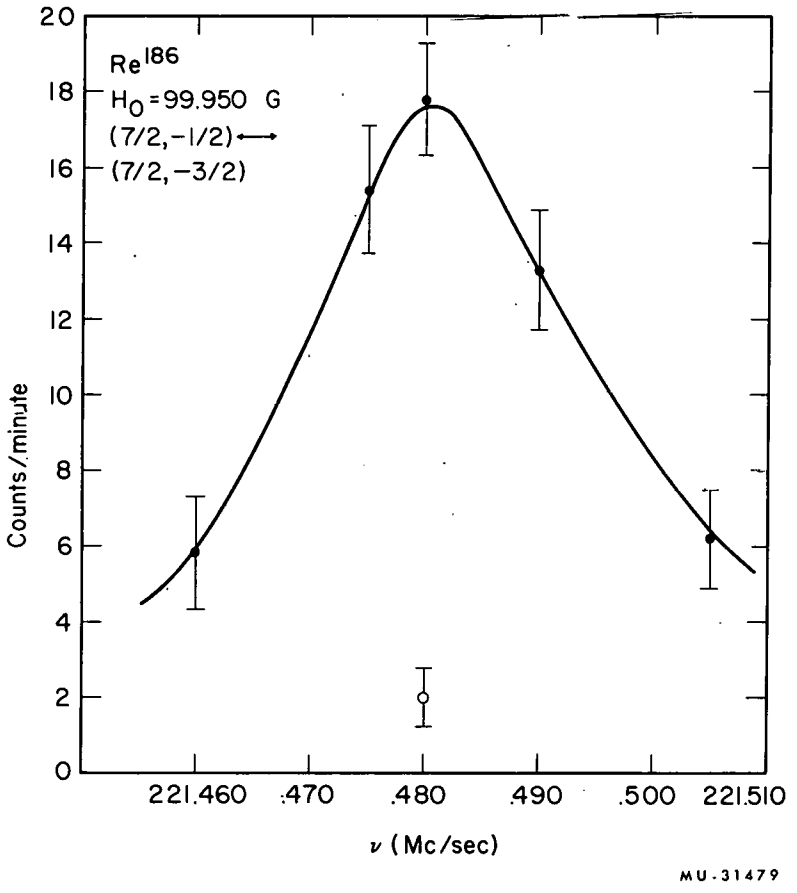

Fig. 30. Alpha transition in Re^{186} at 99.950 G.

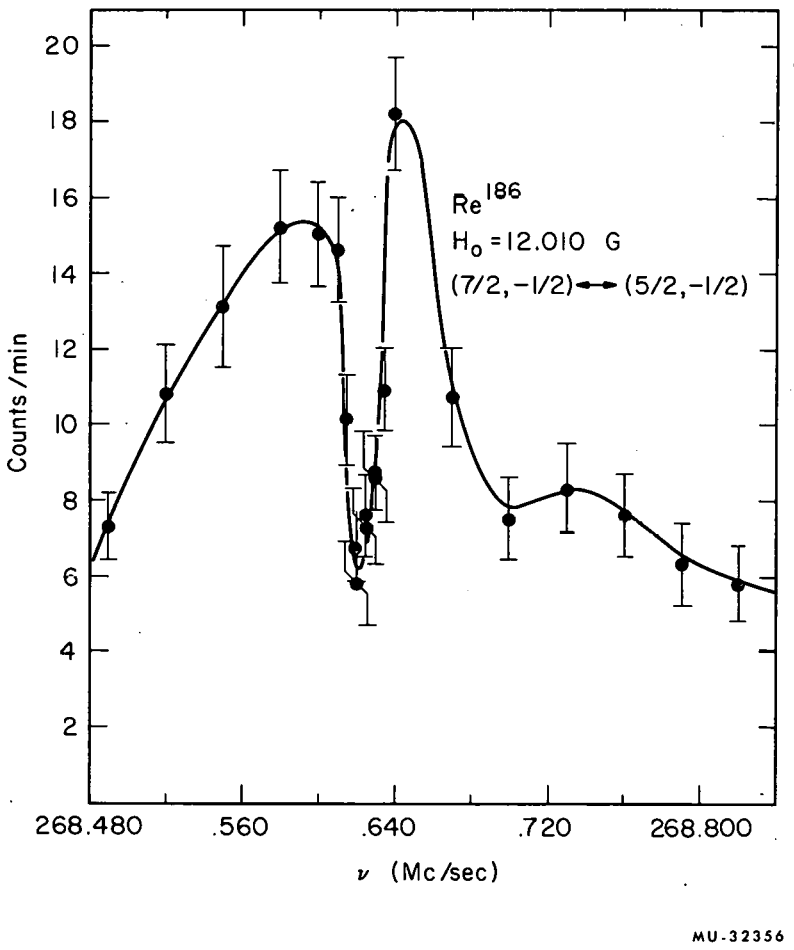

Fig. 31. (7/2, - 1/2) ⟷ (5/2, - 1/2) direct transition in Re^{186} at 12.010 G.

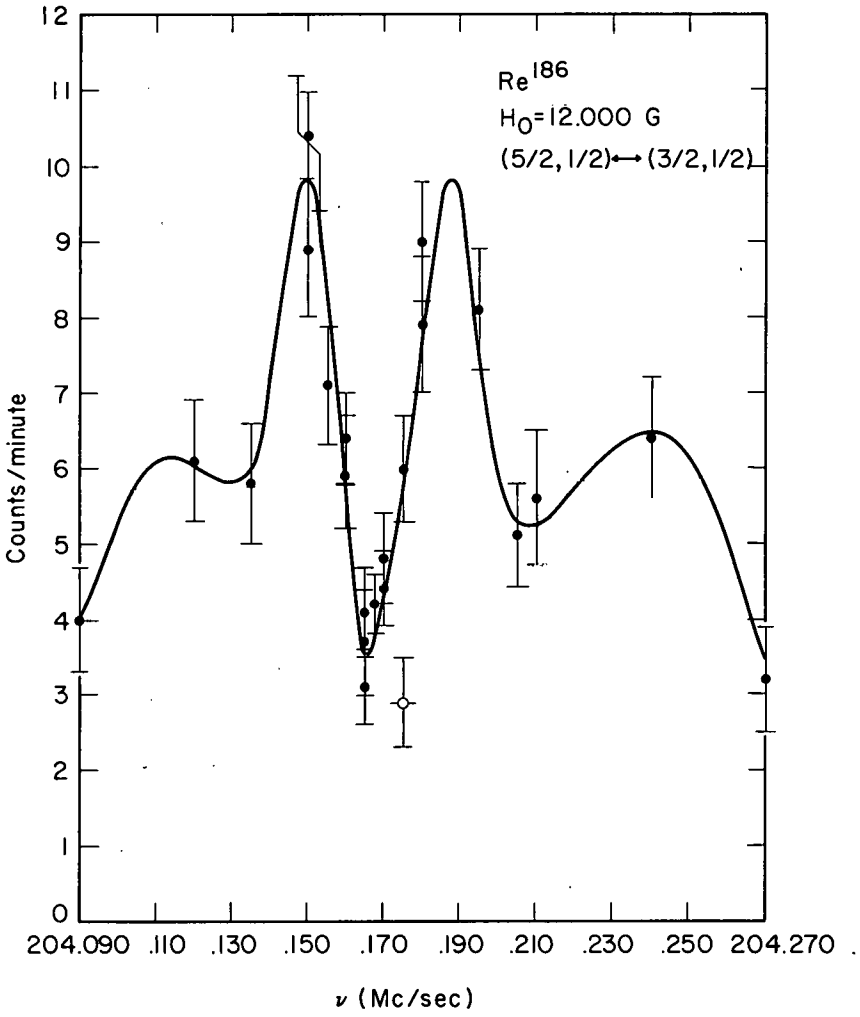

Fig. 32. (5/2, 1/2) ⟷ (3/2, 1/2) direct transition in Re^{186} at 12.000 G.

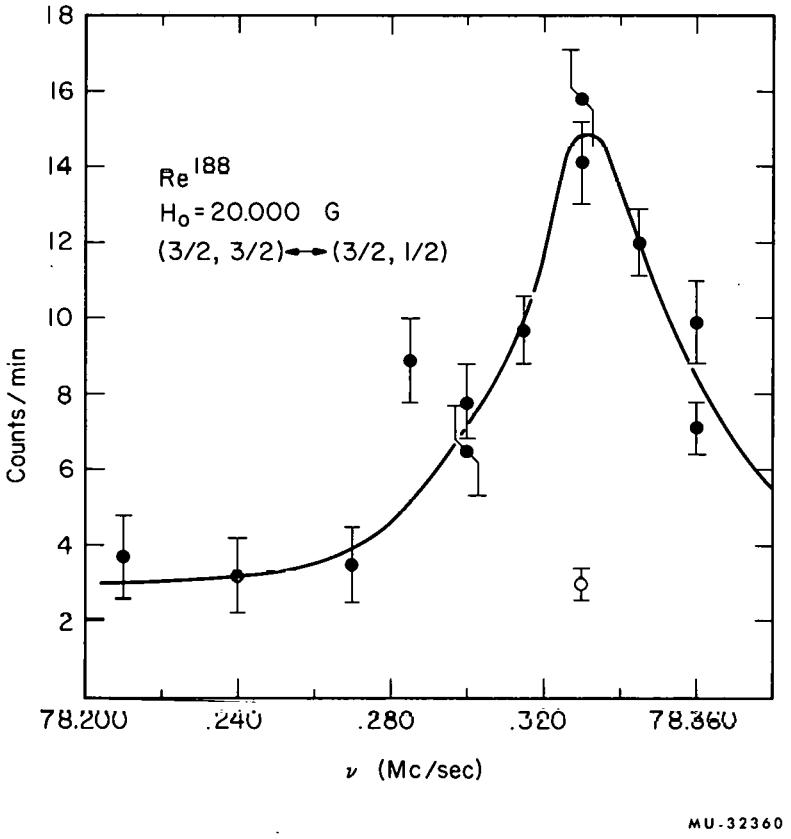

Fig. 33. Gamma transition in Re^{188} at 20.000 G.

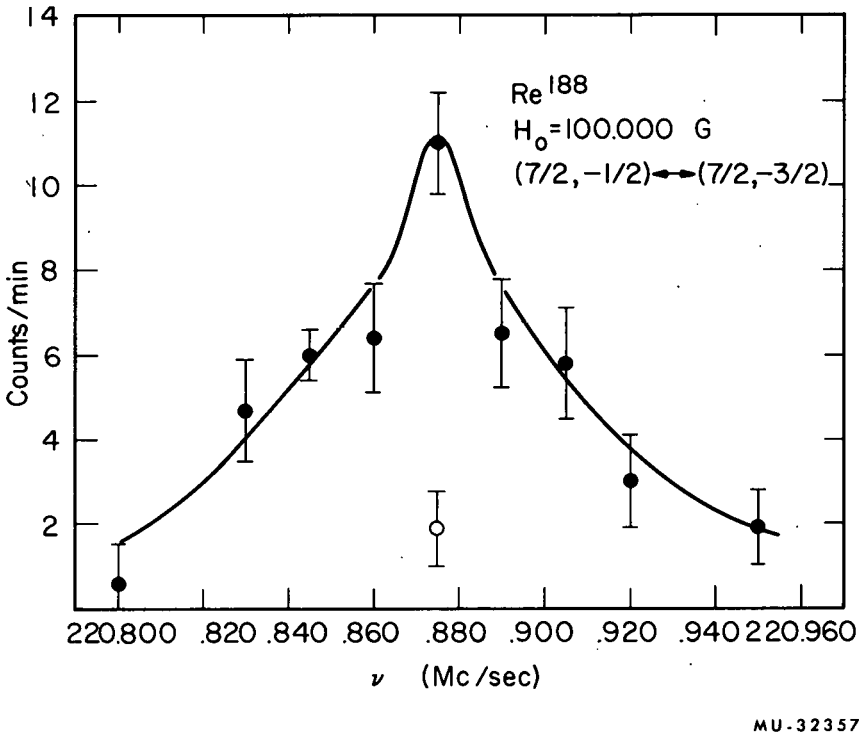

Fig. 34. Alpha transition in Re^{188} at 100.000 G.

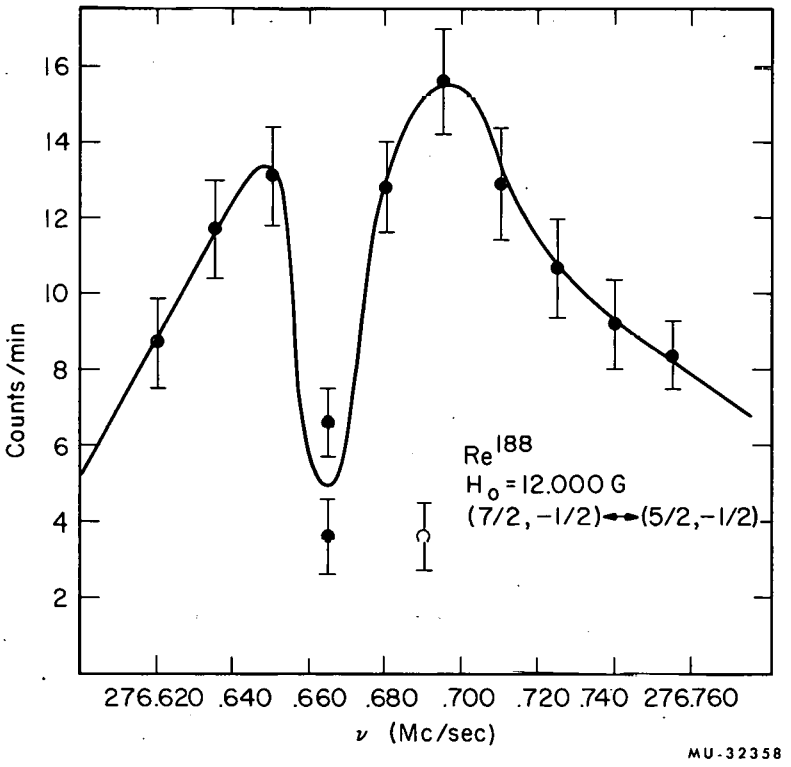

Fig. 35. $(7/2, -1/2) \longleftrightarrow (5/2, -1/2)$ direct transition in Re^{188} at 12.000 G.

Table VI. Re^{186}: Magnetic dipole, electric quadrupole, and g variables.

a	b	g_J	$g_I \times 10^4$	Errcr in a	Error in b	Error in g_J	Error in $g_I \times 10^4$	χ^2
78.3058	-8.3601	-1.951997	11.444159	0.0012	0.0025	0.000044	6.939246	1.3444083

Energy levels and residuals

b/a = -0.1068

μ/h = 1.399677

M_p/M_e = 1836.12

μ_I = 2.101285

Run No.	Frequency (Mc/sec)	Residual (Mc/sec)	Freq. error (Mc/sec)	F_1	M_1	F_2	M_2	H (G)	ΔH (G)	Weight factor
1	129.9300	0.0152	0.0150	5/2	1/2	5/2	-1/2	50.0003	0.0092	1122.8
2	480.1450	-0.0108	0.0150	7/2	-1/2	7/2	-3/2	200.0000	0.0044	2783.9
3	103.8550	0.0147	0.0150	7/2	-1/2	7/2	-3/2	50.0003	0.0092	1562.9
4	190.8450	0.0109	0.0150	3/2	3/2	3/2	1/2	50.0003	0.0092	810.8
5	78.3350	0.0045	0.0150	3/2	3/2	3/2	1/2	20.0000	0.0119	410.2
6	273.0000	0.0093	0.0150	5/2	1/2	5/2	-1/2	99.9995	0.0064	1807.8
7	221.4800	0.0087	0.0150	7/2	-1/2	7/2	-3/2	99.9499	0.0064	2119.9
8	204.1675	0.0000	0.0050	5/2	1/2	3/2	1/2	11.9999	0.0128	39862.6
9	268.6220	-0.0003	0.0070	7/2	-1/2	5/2	-1/2	12.0102	0.0128	14980.9

Table VII. Re^{188}: Magnetic dipole, electric quadrupole, and g variables.

a	b	g_J	$g_I \times 10^4$	Error in a	Error in b	Error in g_J	Error in $g_I \times 10^4$	χ^2
80.4320	-7.7455	-1.952082	3.190500	0.0016	0.0030	0.000075	6.597555	0.38542005

Energy levels and residuals

$b/a = -0.0963$

$\mu/h = 1.399677$

$M_p/M_e = 1836.12$

$\mu_I = 2.421934$

Run No.	Frequency (Mc/sec)	Residual (Mc/sec)	Freq. error (Mc/sec)	F_1	M_1	F_2	M_2	H (G)	ΔH (G)	Weight factor
1	39.8850	0.0110	0.0150	7/2	-1/2	7/2	-3/2	20.0000	0.0119	1224.4
2	51.1350	0.0087	0.0150	5/2	1/2	5/2	-1/2	20.7547	0.0118	884.6
3	129.7250	-0.0041	0.0150	5/2	1/2	5/2	-1/2	50.0003	0.0092	1125.2
4	78.3300	0.0081	0.0150	3/2	3/2	3/2	1/2	20.0000	0.0119	409.8
5	191.2100	-0.0072	0.0150	3/2	3/2	3/2	1/2	50.0003	0.0092	802.2
6	272.9000	0.0037	0.0150	5/2	1/2	5/2	-1/2	99.9995	0.0064	1803.1
7	220.8750	-0.0008	0.0150	7/2	-1/2	7/2	-3/2	99.9995	0.0064	2129.8
8	103.6270	-0.0060	0.0150	7/2	-1/2	7/2	-3/2	50.0003	0.0092	1570.5
9	276.6650	-0.0001	0.0100	7/2	-1/2	5/2	-1/2	11.9999	0.0128	8548.5
10	208.4850	0.0000	0.0050	5/2	1/2	3/2	1/2	11.9999	0.0128	39973.2

Taking the weighted average of the two values obtained for g_J, we obtain the value

$$g_J = 1.95203(8) .$$

For pure Russell-Saunders coupling, the g_J factor is given by[49]

$$g_J = 1 + (g_s - 1)\frac{J(J+1) + S(S+1) - L(L+1)}{2J(J+1)} . \qquad (6.3)$$

Therefore, the g_J value for rhenium should be

$$g_J = g_s = -2.00229 .$$

The major part of the discrepancy between this value and the experimental value should come from the breakdown of Russell-Saunders coupling.

The terms which arise from five equivalent d electrons are given by Condon and Shortley[1] and are

$$^2SPDFGHI \qquad ^4PDFG \qquad ^6S .$$

The only states that the fine-structure interaction can couple are the states whose quantum numbers differ by $\Delta L = 0 \pm 1$, $\Delta S = 0 \pm 1$, and $\Delta J = 0$. In order to include second-order effects, we can write the angular part of the ground-state wave function as a linear combination of the ^6S, ^4P, and ^4D terms as

$$\left|J = 5/2, m_J\right\rangle = (1 - \alpha^2 - \beta^2)^{1/2}\left|^6S_{5/2}, m_J\right\rangle + \alpha\left|^4P_{5/2}, m_J\right\rangle + \beta\left|^4D_{5/2}, m_J\right\rangle .$$

The constants α and β are determined from the diagonalization of the matrix of the spin-orbit energy, $\sum_i a_{5d}\, \underset{\sim}{l}_i \cdot \underset{\sim}{s}_i$, plus the electrostatic energy, $\sum_{i>j} e^2/r_{ij}$. The unitary matrix that transforms the matrix to diagonal form is then used to obtain the wavefunction. Incomplete knowledge of the electronic constant can be eliminated by use of the formula

$$g_J = (1 - \alpha^2 - \beta^2)g_J(^6S_{5/2}) + \alpha^2 g_J(^4P_{5/2}) + \beta^2 g_J(^4D_{5/2}) .$$

Using this wavefunction, we can then determine the magnetic-dipole interaction constant, a, and the electric quadrupole interaction

constant, b, by calculating

$$a = - \frac{\mu_I \langle JJ | H_z | JJ \rangle}{IJ} ,$$

where

$$H_z = - 2\mu_0 \sum_i \left(\frac{1}{r_i}\right)^3 \left[\ell_z - s_z + \frac{3}{2r^2} [z(\underset{\sim}{s} \cdot \underset{\sim}{r}) + (\underset{\sim}{s} \cdot \underset{\sim}{r})z] \right]_i ,$$

and

$$b = - e^2 Q \left\langle JJ \middle| \sum_i \left[\frac{(3 \cos^2 \theta - 1)}{r^3} \right]_i \middle| JJ \right\rangle .$$

Configuration interaction, particularly of configurations that have unpaired s electrons, can contribute appreciably to the hyperfine structure of an atom. However, this is much more difficult to calculate and only rough approximations are usually done.

From Eq. (2.11) we see that, since $c = 0$,

$$W_{7/2} = 5/2\ a + 1/4\ b ,$$

$$W_{5/2} = - a - 4/5\ b ,$$

and

$$W_{3/2} = - 7/2\ a + 7/10\ b .$$

Therefore from Eq. (2.12) we obtain, for the two hyperfine-structure separations,

$$\Delta\nu(7/2, 5/2) = 7/2\ a + 21/20\ b$$

and

$$\Delta\nu(5/2, 3/2) = 5/2\ a - 3/2\ b .$$

From this we obtain for the hyperfine-structure separations of Re^{186} the values

$$\Delta\nu_{186}(7/2, 5/2) = \pm 265.292(14)\ Mc/sec$$

and

$$\Delta\nu_{186}(5/2, 3/2) = \pm 208.305(14)\ Mc/sec .$$

For Re^{188} we obtain the values

$$\Delta\nu_{188}(7/2, 5/2) = \pm 273.379(13) \text{ Mc/sec}$$

and

$$\Delta\nu_{188}(5/2, 3/2) = \pm 212.698(17) \text{ Mc/sec} .$$

ACKNOWLEDGMENTS

I thank the many people involved in bringing this research to a successful conclusion, especially:

Professor William A. Nierenberg for his support.

Professor Howard A. Shugart for initially stimulating in me an interest in atomic-beam work and for his ability to give science a personal touch.

Dr. Douglas McColm for his patience with a "green" graduate student and his continued guidance throughout this research.

Dr. Matthew B. White for his assistance and the pleasure of many enlightening discussions.

Mr. Douglas Macdonald for his engineering aid.

Mr. Robert McCracken for expediting the radioactive samples.

The Health Chemistry monitors for their assistance in handling the radioactive samples.

Miss Christina Frank for typing the manuscript.

Finally, my wife, Alison for sharing the varied experiences of graduate school with me and for her continuing confidence in me.

This work was done under the auspices of the U. S. Atomic Energy Commission.

APPENDIX

The Magnetic Field at the Nucleus Due to a Spherical Spin Distribution

For pure Russell-Saunders coupling the magnetic field at the nucleus is given by[49]

$$\underset{\sim}{H} = -2\mu_0 \left[\underset{\sim}{L} - \underset{\sim}{S} + 3\underset{\sim}{r}\,(\underset{\sim}{S}\cdot\underset{\sim}{r})/r^2\right] 1/r^3 .$$

Since the electronic ground state of rhenium is an S state, the magnetic field at the nucleus due to the electronic spin moment at $\underset{\sim}{r}$ is

$$\underset{\sim}{H} = 2\mu_0 \left[\underset{\sim}{S} - 3\underset{\sim}{r}\,\underset{\sim}{S}\cdot\underset{\sim}{r}/r^2\right] 1/r^3 .$$

Choosing a coordinate system whose z axis is along $\underset{\sim}{S}$, we have

$$\underset{\sim}{H}(r,\theta,\phi) = 2\mu_0/r^3 \left[S\,(1 - 3\cos^2\theta)\,\underset{\sim}{e}_z - 3S\cos\theta\sin\theta\cos\phi\,\underset{\sim}{e}_x - 3S\cos\theta\sin\theta\sin\phi\,\underset{\sim}{e}_y\right] .$$

Now, since the ground state of rhenium is spherically symmetric (S state), the magnetic field at the nucleus due to a thin spherical shell of radius r is

$$\underset{\sim}{H}(r) = \int \underset{\sim}{H}(r,\theta,\phi)\,d\Omega$$

$$= \frac{2\mu_0}{r^3} S\left[\underset{\sim}{e}_z \int_0^{2\pi}\int_0^{\pi} (1 - 3\cos^2\theta)\sin\theta\,d\theta\,d\phi\right.$$

$$- 3\,\underset{\sim}{e}_x \int_0^{2\pi}\int_0^{\pi} \cos\theta\sin^2\theta\cos\phi\,d\theta\,d\phi$$

$$\left. - 3\,\underset{\sim}{e}_y \int_0^{2\pi}\int_0^{\pi} \cos\theta\sin^2\theta\sin\phi\,d\theta\,d\phi\right] .$$

Since

$$\int_0^{2\pi} \cos\phi\,d\phi = \int_0^{2\pi} \sin\phi\,d\phi = \int_0^{\pi} \cos\theta\sin^2\theta\,d\theta = 0,$$

we have

$$\underset{\sim}{H}_x(r) = \underset{\sim}{H}_y(r) = 0 .$$

Also, we have

$$\int_0^{\pi} \sin\theta \, d\theta = 2 ,$$

and

$$\int_0^{\pi} \cos^2\theta \sin\theta \, d\theta = 2/3 .$$

Thus, we obtain $\underset{\sim}{H}_z = 0$.

Therefore, we have $\underset{\sim}{H}(r) = 0$, and, since each shell contributes zero field at the nucleus, the total magnetic field from a spherical state is zero.

REFERENCES

1. E. U. Condon and G. H. Shortley, The Theory of Atomic Spectra (Cambridge University Press, Cambridge, England, 1957).
2. C. Schwartz, Phys. Rev. 97, 380 (1955).
3. M. Rotenberg, R. Bivins, N. Metropolis, and J. Wooten, Jr., The 3-j and 6-j Symbols (The Technology Press, Massachusetts Institute of Technology, Cambridge, Massachusetts, 1959).
4. G. Breit and I. I. Rabi, Phys. Rev. 38, 2082 (1931).
5. N. F. Ramsey, Molecular Beams (Oxford University Press, London, England, 1956).
6. E. Fermi, Z. Physik 60, 320 (1930).
7. J. G. King and J. R. Zacharias, "Some New Applications and Techniques of Molecular Beams," in Advances in Electronics and Electron Physics, Vol. VIII (Academic Press, New York, 1956), pp. 1-88.
8. W. A. Nierenberg, Ann. Rev. Nucl. Sci. 7, 349 (1957).
9. H. Kopfermann, Nuclear Moments, English trans. by E. E. Schneider (Academic Press, New York, 1958).
10. E. Fermi and E. Segrè, Z. Physik 82, 729 (1933).
11. H. B. G. Casimir, On the Interaction Between Atomic Nuclei and Electrons (Teyler's Tweede Gnootschap, Haarlem, Holland, 1936).
12. J. E. Rosenthal and G. Breit, Phys. Rev. 41, 429 (1932).
13. M. F. Crawford and A. L. Schawlow, Phys. Rev. 76, 1310 (1949).
14. N. J. Jonesco-Pallas, Phys. Rev. 117, 505 (1960).
15. A. Bohr and V. F. Weisskopf, Phys. Rev. 77, 94 (1950).
16. A. Bohr, Phys. Rev. 81, 331 (1951).
17. G. Breit and R. E. Meyerott, Phys. Rev. 72, 1023 (1947).
18. H. A. Bethe and E. E. Salpeter, Quantum Mechanics of One- and Two-Electron Systems, in Handbuch der Physik, Vol. XXXV (Springer-Verlag, Berlin, Germany, 1957), pp. 88-436.
19. I. I. Rabi, J. R. Zacharias, S. Millman, and P. Kusch, Phys. Rev. 53, 318 (1938).

20. J. R. Zacharias, Phys. Rev. 61, 270 (1942).

21. R. A. Marrus and W. A. Nierenberg, On Atomic Beams, in Proceedings of the International School of Physics, Enrico Fermi, Course XVII, August 1960 (Academic Press, New York, 1962), pp. 118-156.

22. K. F. Smith, Molecular Beams (Methuen Press, London, England, 1955).

23. M. B. White, Hyperfine Structures and Nuclear Moments of Lu^{176m}, Br^{80}, Br^{80m}, and I^{132} (Ph. D. Thesis), Lawrence Radiation Laboratory Report UCRL-10321, September 1962 (unpublished).

24. A. Bohr, Phys. Rev. 73, 1109 (1948).

25. F. Low, Phys. Rev. 77, 361 (1950).

26. E. N. Adams II, Phys. Rev. 81, 1 (1951).

27. P. Kusch and A. K. Mann, Phys. Rev. 76, 707 (1949).

28. P. Kusch and H. Taub, Phys. Rev. 75, 1477 (1949).

29. N. F. Ramsey, Phys. Rev. 76, 996 (1949).

30. N. F. Ramsey, Phys. Rev. 78, 695 (1950).

31. N. F. Ramsey and H. B. Silsbee, Phys. Rev. 84, 506 (1951).

32. Melvin Klein (Lawrence Radiation Laboratory, Livermore, California), (private communication).

33. W. M. Doyle, Hyperfine-Structure Studies of Er^{169} and Isotopes of Refractory Elements (Ph. D. Thesis), Lawrence Radiation Laboratory Report UCRL-10609, January 1963 (unpublished).

34. W. F. Meggers, J. Res. Natl. Bur. Std. 6, 1027, R. P. 322 (1931).

35. M. A. Preston, Physics of the Nucleus (Addison-Wesley Publishing, Reading, Massachusetts, 1962).

36. A. Bohr, Kgl. Danske Videnskab. Selskab, Mat.-fys. Medd. 26, No. 14 (1952).

37. A. Bohr and B. R. Mottelson, Kgl. Danske Videnskab. Selskab, Mat.-fys. Medd. 27, No. 16 (1953).

38. S. G. Nilsson, Kgl. Danske Videnskab. Selskab, Mat.-fys. Medd. 29, No. 16 (1955).

39. B. R. Mottelson and S. G. Nilsson, Kgl. Danske Videnskab. Selskab, Mat.-fys. Skritter. 1, No. 8 (1959).

40. G. O. Brink, Nuclear Spins of Thallium-197, Thallium-198m, Thallium-199, and Thallium-204 (Ph. D. Thesis), University of California Radiation Laboratory Report UCRL-3642, June 1957 (unpublished).

41. H. L. Garvin, Nuclear-Spin and Hyperfine-Structure Measurements on the Radioactive Iodine and Astatine Isotopes (Ph. D. Thesis), Lawrence Radiation Laboratory Report UCRL-8860, August 1959 (unpublished).

42. R. Marrus, W. A. Nierenberg, and J. Winocur, Phys. Rev. 120, 1429 (1960).

43. P. G. H. Sandars and G. K. Woodgate, Proc. Roy. Soc. (London) A257, 269 (1960).

44. W. M. Doyle and R. Marrus, Bull. Am. Phys. Soc. 7, 605 (1962).

45. H. L. Garvin, T. M. Green, E. Lipworth, and W. A. Nierenberg, Phys. Rev. 116, 393 (1959).

46. W. A. Nierenberg, University of California Radiation Laboratory Report UCRL-3816, June 1957 (unpublished).

47. L. L. Marino, Some Nuclear Properties of Bi^{206}, Tl^{200}, Th^{201} Th^{202}, In^{109}, In^{110m}, and In^{111} (Ph. D. Thesis), Lawrence Radiation Laboratory Report UCRL-8721, April 1959 (unpublished).

48. R. A. Fisher, Statistical Methods for Research Workers (Hafner, New York, 1958).

49. B. R. Judd, Operator Techniques in Atomic Spectroscopy (McGraw-Hill, New York, 1963).

This report was prepared as an account of Government sponsored work. Neither the United States, nor the Commission, nor any person acting on behalf of the Commission:

A. Makes any warranty or representation, expressed or implied, with respect to the accuracy, completeness, or usefulness of the information contained in this report, or that the use of any information, apparatus, method, or process disclosed in this report may not infringe privately owned rights; or

B. Assumes any liabilities with respect to the use of, or for damages resulting from the use of any information, apparatus, method, or process disclosed in this report.

As used in the above, "person acting on behalf of the Commission" includes any employee or contractor of the Commission, or employee of such contractor, to the extent that such employee or contractor of the Commission, or employee of such contractor prepares, disseminates, or provides access to, any information pursuant to his employment or contract with the Commission, or his employment with such contractor.